Cooperative domain structures in highly anisotropic alloys with twinned microstructure

N. I. Vlasova, G. S. Kandaurova, L. G. Onoprienko, and N. N. Shchegoleva

Institute of Metal Physics Ural Branch of the Russian Academy of Sciences; Ural State University, Ekaterinburg; Russian Scientific Research Center for Microelectronics Technology, Moscow

(Submitted 19 December 1991)
Usp. Fiz. Nauk **162**, 161–197 (May 1992)

1. INTRODUCTION

There exists a large class of highly anisotropic ferromagnets that have a regularly nonuniform microcrystalline structure. These magnets include their alloys Co–Pt, Fe–Pt, and Fe–Pd with type $L\,1_0$ ordering. Because of the fortunate combination of superior magnetic, mechanical and anticorrosion properties, these alloys are used as materials for permanent magnets. During ordering, a face-centered tetragonal phase is formed out of the high-temperature *fcc* phase. The face-centered tetragonal (*fct*) phase is a highly anisotropic magnetically uniaxial phase ($K = 2$–7 kJ/m^3 and $M_s = 800$–1150 kA/m) with the easy axis along the tetragonal c axis.[1–4] It is noteworthy that the ordered phase consists of regular systems (blocks, plates, stacks) of crystalline domains of twinned orientation, the so-called c-domains.[5–13] Neighboring c-domains, which have the form of thin plates of thickness $d = 0.01$–$0.1\,\mu$m, are coherently joined together along one of the $\{101\}$ planes so that the tetragonal c axis (the easy axis) is misoriented by an angle $2\alpha = \pi/2$. The thickness of the c-domains and the shape and size of the regular twinned systems depend on the relation between the rate of formation and the rate of growth of the nuclei of the ordered structure in the *fcc–fct* phase transition.[14]

From an analysis of the experimental data it is found that alloys that are ordered by different means differ sharply in the coercive force H_c and relative residual magnetization $j_r = M_r/M_s$ (compare, e.g., Refs. 1 and 13). The best hysteresis properties are obtained for states where the alloy contains a predominantly ordered phase in the form of thin plates of c-domains.[15] The large difference in H_c and j_r among the alloys with different sizes of the c-domains cannot be explained consistently in terms of only the misorientation of the easy axis, the degree of dispersion, or the magnetic independence of the c-domains. In view of this situation, a microscopic magnetic theory of twinned systems was developed in Refs. 16–21, with allowance for exchange and magnetostatic interactions at the twin boundaries. The presence of the exchange interaction has been demonstrated experimentally in Ref. 21.

It follows from the microscopic magnetic theory that, because of these interactions, magnetic domain walls of the Neél type are formed in a twinned system; they are pinned at the twin boundaries, and under magnetization reversal, metastable magnetic states appear. Kandaurova *et al.*[16] have calculated the critical fields for which the internal structure of the "frozen-in" magnetic walls undergoes reorganization as a result of an irreversible change in orientation of the magnetization in the c-domains in a magnetic field. In the model of coherent rotation of the **M** vectors we have calculated the hysteresis properties of a twinned system taking into account the magnetostatic interaction.[22–24] Although these calculations show that the hysteresis characteristics are considerably degraded as compared to the case of a ferromagnet that is uniform over the crystal structure, the experimentally observed maximum values of H_c are much lower than predicted by the theory. This means that reversal of magnetization of an alloy with a twinned microstructure takes place not by the rotation of the magnetization vectors **M**, but by the formation and displacement of 180° domain walls.

In this paper we present a summary of the results of systematic investigations of the magnetic domain structure in ordered alloys with twinned systems of various degrees of dispersion in the absence of a magnetic field and the results of a study of the behavior of these materials in a magnetic field. We show that the exchange and magnetostatic interactions at the boundaries of the c-domains lead to the formation of a special type of domain structure, a cooperative macrodomain magnetic structure. Below, we describe the more characteristic features of such a domain structure.

2. FEATURES OF THE MICROSTRUCTURE AND MAGNETIC PROPERTIES

Because of the specific orientation relation between the *fcc* and *fct* phases[25] any surface of an initially disordered single-crystal that undergoes the *fcc–fct* phase transition can exhibit a variety of cross sections of regular twinned systems. We shall call such a crystal a "poly-twinned" crystal. As an example, Fig. 1 shows a picture of portions of the microstructure of poly-twinned crystals of FePt (Fig. 1a,b) and CoPt (Fig. 1c,d). The thickness of the c-domains, as well as the shape and size of the regular twinned systems depend on the relation between the rate of formation of nuclei of the ordered structure and the rate of growth of the ordered structures. For massive crystals that are ordered near the phase transition temperature T_c (the rate of growth of the nuclei is high), the tetragonal phase is typically formed as stacks of poly-twinned plates. The c-domains in a plate and the plates in a stack are joined together by various junction planes of type $\{110\}$. A stack that has grown out from a single center of ordering is distinguished by the common direction of the boundaries of the c-domains that form it on the junction plane of the poly-twinned plates. In the equivalent FePt alloy these macroscopically regular twinned systems are formed even after quick quenching in water, because of the very high critical temperature $T_c = 1300$ °C (Fig. 1a,b). The c-domains are some tenths of a micron thick, and the dimension L_1 of a plate and L of a stack varies between 1 and 10 μm and between 10 and 100 μm, respectively. The diagram shown in Fig. 2a may serve to interpret

 0038-5670/92/050420-19$03.00

the portion of the microstructure of the (001) surface of a FePt crystal shown in Fig. 1b.

In the alloy CoPt it is possible the form regular twinned systems of various degrees of dispersion ($T_c = 830\,°C$). Since the rate of formation of *fct* nuclei is high, the tendency for formation of poly-twinned plates is found here too, but in this case the plates have a block structure and only blocks of *c*-domains comprise the regular twin systems. Each block consists of two kinds of coherently joined *c*-domains. Figure 1c,d shows for comparison portions of the microstructures of poly-twinned crystals, ordered by different means. It can be seen that the crystals are quite different in the size of the blocks and the thickness of the *c*-domains. After quenching and annealing at 660 °C the blocks of *c*-domains are extremely small (Fig. 1d), and are comparable in size to the *c*-domains themselves. The *c*-domains are hundredths of a micron thick and the blocks of *c*-domains tenths of a micron. Adjacent *c*-domains differ in the orientation of the planes at which the *c*-domains are joined and in the orientation of the tetragonal *c* axes.

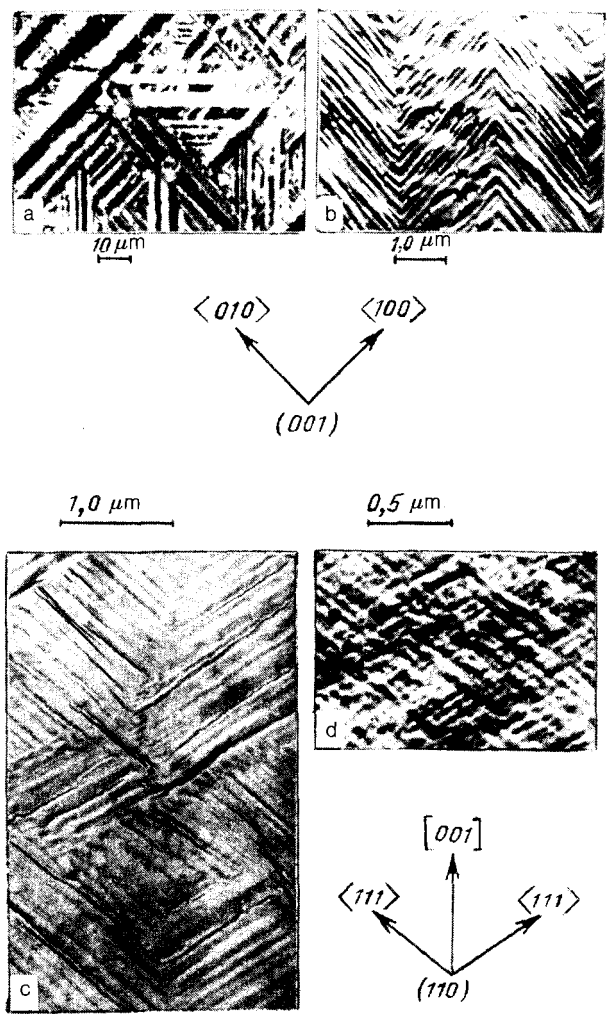

FIG. 1. Microstructure of FePt and CoPt crystals revealed by (a) an optical microscope and (b) an electron microscope (b–d) with the use of carbon replicas; a,b) on the (001) FePt crystal surface after quenching in water from 1300 °C; c) on the (110) CoPt surface after cooling from 850 to 750 °C for 6 h and then annealing for 4 h at 750 °C; d) on the (110) CoPt surface after quenching in water from 1000 °C and then annealing for 30 min at 660 °C.

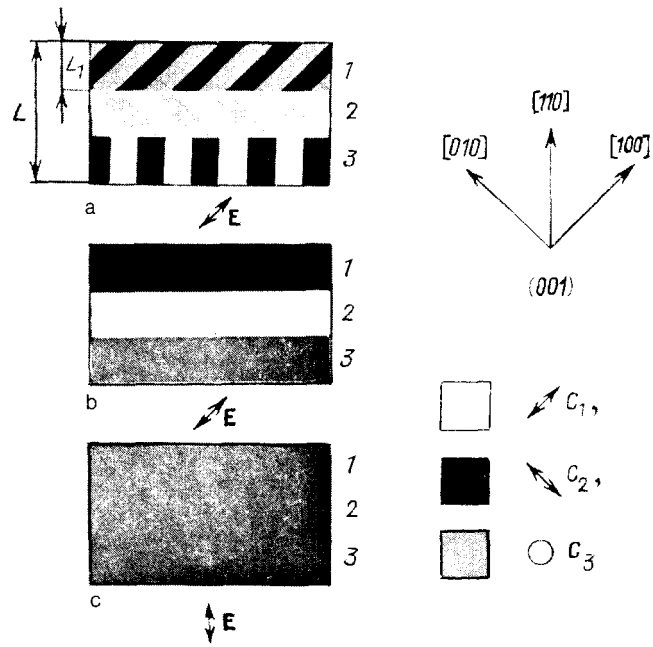

FIG. 2. Schematic diagram of the contrast pattern in polarized light on the (001) surface of an unmagnetized ordered poly-twinned crystal of type CuAuI for various thickness of the *c*-domains and various orientations of the plane of polarization. a) Thickness of the *c*-domains above the limit of resolution of the optical microscope; b,c) Thickness of the *c*-domains below the limit of resolution of the microscope. The different coloring of the *c*-domains corresponds to the different orientations of the tetragonal *c* axis. The orientation of the plane of polarization is given by the vector **E**.

Thus, only blocks of *c*-domains are regular twinned systems.

As shown in Refs. 14, 26, and 27, the intricate structural hierarchy of the ordered *fct* phase (*c*-domains, blocks, plates, stacks) is due to the tendency of the crystal to minimize the elastic energy associated with internal stresses. These stresses arise as a result of the large difference in the lattice parameters of the ordered and the disordered phases in the *fcc–fct* phase transition.[13–15,25] According to electron microscope observations,[6,10,14] the coherent twin boundaries of the *c*-domains contain no dislocations and are free of internal stresses, i.e., they are invariant. Dislocations are concentrated at the boundaries of large plates and stacks that have grown from different centers, and strong internal stresses are found at the coherent boundaries of highly dispersed blocks of *c*-domains.[6,10,14]

The alloys with a high degree of dispersion of the twin systems have large differences in the maximum values of H_c and j_r. For example, for a slowly cooled CoPt alloy near T_c (where the rate of nucleus growth is high), $H_c = 80$ kA/m and $j_r = 0.3$ (Ref. 1). When the rate of formation of nuclei is high (after quenching in water and subsequent annealing at 500–780 °C) the material exhibits superior hysteresis properties. After annealing at 660 °C for 20 min a record high value of the energy product (BH) was obtained for the equiatomic alloy CoPt, $(BH)_{max} = 120\,T\cdot A/m$ at $H_c = 480$ kA/m and $j_r = 0.82$ (Ref. 13). The anisotropy of H_c and j_r are of the form characteristic of multiaxis crystals; the hysteresis loops have a stepped form, and j_r is higher than the values calculated for an ensemble of magnetically uniaxial noninteracting particles with allowance for the distribution

of the orientation of the easy axis. These features of the magnetic properties of poly-twinned crystals are presumably due to the existence of exchange and magnetostriction interactions at the twin boundaries of the c-domains.[21-24]

3. MAGNETIC DOMAIN STRUCTURE OF POLY-TWINNED CRYSTALS IN THE THERMALLY-INDUCED DEMAGNETIZED STATE

3.1. Observed features of the magnetic domain structure

After sample plates of the alloys FePt and CoPt were etched in concentrated hydrochloric acid and mechanically polished in fine diamond paste (10–0.1 μm) the magnetic domain structure was observed by means of a magnetic suspension by the electron-microscope replica method of Craik,[28] and by the polar magneto-optical Kerr effect.[29] The surfaces of the plates, with dimensions $4\times4\times1$ mm coincided with the (001), (110), and (111) planes of the initial unordered crystals. As has been stated above, different cross sections of stacks of poly-twinned plates or blocks of c-domains, formed on all possible $\{110\}$ planes, were observed on the same surface. For the sake of brevity we shall call the junction plane of the poly-twinned plates in a stack the base of the stack, and the planes perpendicular to it or inclined to it, the prismatic and pyramidal planes, respectively.

In interpreting the pattern obtained in polarized light we took into account the superposition of two main effects: the polar magneto-optical Kerr effect and the effect of anisotropic reflection contrast.[5] The latter is due to the elliptical polarization of a linearly polarized light when it reflects from an anisotropic metal surface[30] and it occurs both in magnetic and in nonmagnetic optically anisotropic crystals. If such a crystal is rotated about the optical axis of the microscope the orientation of the plane of polarization of the incident light changes relative to the principal crystallographic axes of the sample, and the intensity of the reflected light varies, going through a maximum and a minimum. If the field of view of the microscope includes two crystals whose tetragonal axes lie in the plane of observation but are mutually misoriented by an angle of $\pi/2$, while the plane of polarization of the light is along one of the c axes, then the contrast between the crystals is a maximum; one is white and the other is black. If the plane of polarization makes an angle of $\pi/4$ with the axes of the crystal, then they are indistinguishable in contrast (they are both gray).

Within this picture, the contrast pattern in polarized light on the (001) surface of a nonmagnetic crystal consisting of stacks of poly-twinned plates with a regular internal structure will have the form shown in Fig. 2a if the size of the c-domains is above the limit of resolution of the optical microscope. Each plate should exhibit a regular alternation of gray and black bands (plate *1*), gray and white bands (plate *2*), or black and white bands (plate *3*), depending on the orientation of the tetragonal axes in the c-domains that form the plate. When this poly-twinned crystal is rotated about the axis of the microscope the intensity of the reflected light will vary in the c-domains with tetragonal c axes parallel to the plane of observation, (these are the white and black bands in Fig. 2a); with a rotation by an angle of $\pi/4$ the contrast between the white and the black c-domains disappears, and for an angle of $\pi/2$ the white domains become black and the black ones white. The color of the c-domains with the tetragonal c axes normal to the surface of observation (see plates *1* and *2*) will not change with rotation since these are optically isotropic parts of the surface.

However, in the experiments with c-domains in ordered poly-twinned crystals there are very small dimensions that are not resolved with the optical microscope.[6-14] It is clear that here the contrast pattern on the poly-twinned plates is formed as a result of the superposition of the intensities of the light reflected from individual c-domains.[30] Then the poly-twinned plates, consisting of gray and black c-domains of equal thickness, will have an overall dark color, while the plate formed of the gray and white c-domains will be light-colored (see plates *1* and *2* in Fig. 2a,b). If the sample is rotated about the axis of the microscope the same change in intensity should be seen on plates with this internal structure (plates *1* and *2* in Fig. 2c) as for the corresponding rotation of a single crystal with an anisotropic surface. For example, Fig. 2b,c shows schematically the contrast pattern on plates *1* and *2* for different configurations of the plane of polarization relative to the tetragonal axes in the c-domains. It is interesting to note that the overall intensity of the reflected light for plates that contain dispersed c-domains of equal thickness with the c axes parallel to the plane of observation, but misoriented by $\pi/2$, remains the same as for different orientations of the plane of polarization. Therefore, when the crystal is rotated the gray color of these plates remains (see plate *3* in Fig. 2b,c). We have in fact seen this variation in the pattern of the contrast in polarized light on the (001) surface of a nonmagnetic poly-twinned CuAu crystal.[31]

A ferromagnetic uniaxial crystal exhibits, in addition to the anisotropic reflection contrast, the polar magneto-optical Kerr effect, which consists of a rotation of the plane of polarization of the light as it is reflected from a surface magnetized along the normal. We shall henceforth arbitrarily regard a c-domain with the c axis normal to the surface as being colored white if the magnetization vector **M** in the c-domain is directed upward along the normal to the observed surface ($\odot$) and black if the vector **M** is oriented in the opposite direction ($\oplus$). At the reflecting surface of a nonmagnetic crystal the c-domains with this tetragonal c axis always appeared gray in polarized light (Fig. 2a, plates *1* and *2*).

The contrast pattern in polarized light at one or another surface of a ferromagnetic poly-twinned crystal will depend on the size of the elements of the microstructure, the orientation of the tetragonal axes relative to the surface of observation, the plane of polarization of the light, and the direction of the magnetization vector in the c-domains with a normal c axis. For example, if the distribution of the magnetization in a stack of poly-twinned plates on the (001) surface corresponds to Fig. 3a, and the thickness of the c-domains and of the poly-twinned plates is above the resolution limit of the optical microscope, then the contrast pattern will look like that shown schematically in Fig. 3b (the plane of polarization is indicated by the arrows). If the thickness of the c-domains, for the same plate size, is below the resolution of the microscope, then the contrast pattern, as noted above, is formed by a superposition of the light reflected from the individual c-domains. For this case Fig. 3c,d shows the contrast pattern on the surface of the same stack as in Fig. 3b for two orientations of the plane of polarization. We have observed similar contrast patterns for poly-twinned FePt and

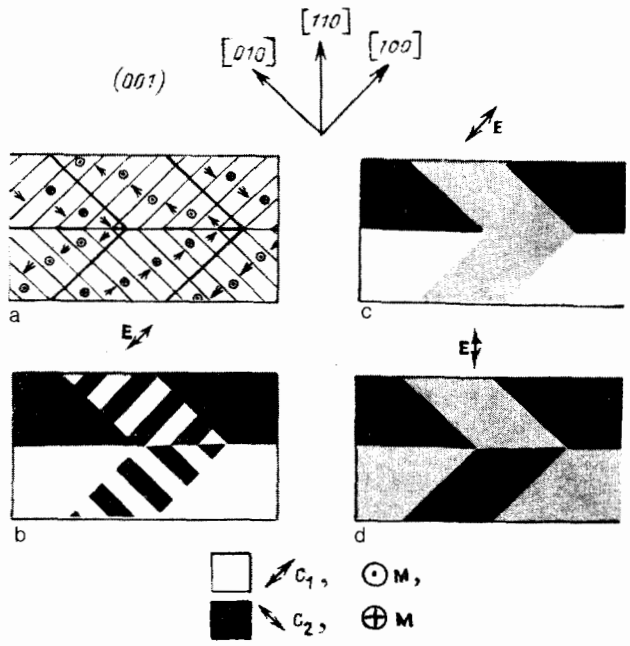

FIG. 3. Schematic diagram of the contrast pattern on the (001) surface of a ferromagnetic poly-twinned crystal for a specified distribution of the magnetization vectors **M** in the *c*-domains and various orientations of the plane of polarization relative to the tetragonal axis. a) Distribution of the magnetization in a stack of plates; the thin lines show the boundaries of the *c*-domains, and the heavy lines the 180° magnetic domain walls; the orientation of the magnetization vector **M** relative to the surface of observation is denoted by ↑ ↓, parallel to, and ⊙ ⊕, perpendicular up and down, respectively. b) Contrast pattern for a *c*-domain thickness *d* above the limit of resolution of the microscope; the *c*-domains with different orientations of **M** have different colors. c,d) Contrast pattern for thicknesses of *c*-domains below the limit of resolution. The orientation of the plane of polarization is denoted by the vector **E**.

CoPt crystals.[31] Some of them are shown in Fig. 4 (compare Figs. 4a–c and 3c,d).

Because of the strong anisotropy of the reflection contrast and its superposition with the polar magneto-optical Kerr effect, the same distribution of the magnetization in a poly-twinned crystal can correspond to several contrast patterns. The variation in contrast with rotation of the sample about the optical axis of the microscope is due to *c*-domains with tetragonal *c* axes parallel to the surface of observation. For a fixed position of the sample the contrast pattern varies as a result of the reorientation of the magnetization vector **M** in the *c*-domains with the tetragonal *c* axes normal to the surface of observation. A magnetic domain structure appears in its true form only when there is no anisotropic contrast, i.e., when the plane of polarization of the light makes an angle of $\pi/4$ with the tetragonal axes (Fig. 3d). The behavior described above in the formation of the contrast pattern in polarized light has been used in our work to interpret the complicated microdomain and macrodomain magnetic structure of poly-twinned crystals.

3.2. Domain structure of crystals consisting of large stacks of plates

Figure 4 shows typical patterns of magnetic domain structure on the {100} and {110} surfaces of a poly-twinned FePt crystal consisting of large stacks of poly-twinned plates with a microstructure regular on the macroscopic scale. To each cross section of a stack of plates corresponds its own completely oriented configuration of magnetic domain structure, in which one can distinguish main and secondary (surface) domains. On the basis plane of the stacks the main domains have the form of bands, oriented along the ⟨111⟩

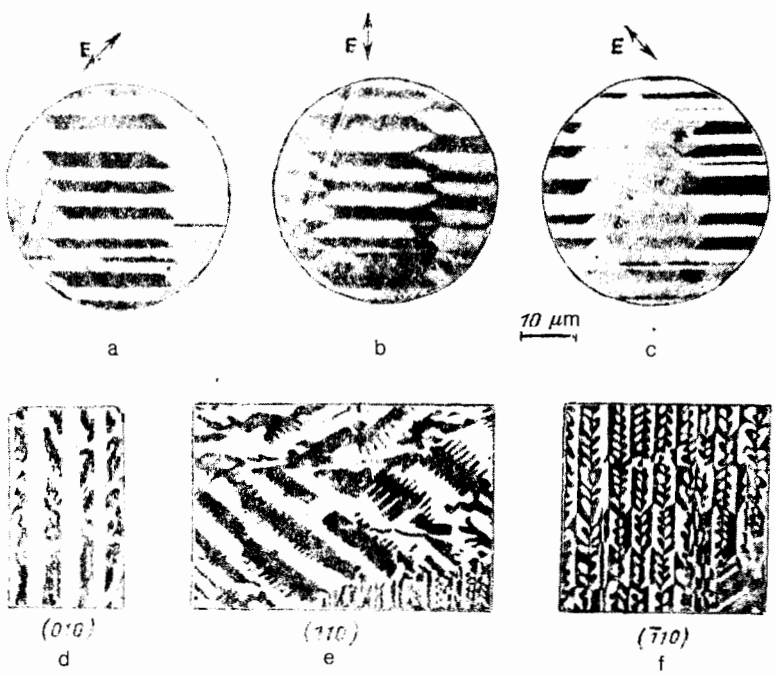

FIG. 4. Magnetic domain structure of a poly-twinned crystal of FePt revealed by means of the polar Kerr magneto-optical effect for different planes of the stacks of poly-twinned plates. a–c) The same spot on the (001) prismatic surface for various orientations of the plane of polarization. d) The pyramidal (010) plane. e) The basal (110) plane. f) The prismatic (110) plane [the (001) plane for Fig. 4b].

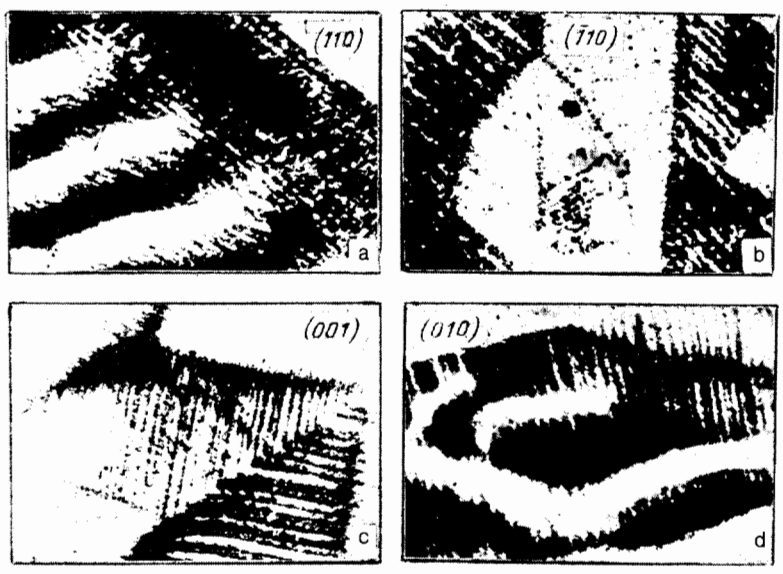

FIG. 5. Magnetic domain structure of a poly-twinned FePt crystal, revealed by means of a Craik replica for the same planes of the stacks as in Fig. 4. a) (110); b) (110); c) (001); d) (010).

directions with an additional structure of "combs" (Fig. 4e). The prismatic cross sections of the stacks have main domains of a zigzag form (Fig. 4a–c,f). The zigzag angle is frequently close to $\pi/2$, but can vary considerably along the normal to the base of the stack. The domain structure does not appear at all in every other alternating plate in the (010) cross section (Fig. 4d). As has been stated above, (Sec. 3.1), these plates consist of c-domains with tetragonal c axes lying in the plane of observation, and they do not contribute to the polar magneto-optical Kerr effect. The nonbasal cross sections of the packets are also distinguished by the configuration of the surface magnetic domains (Fig. 4d,f).

Above all, we note the most characteristic feature of the observed domain structures. Whereas the thickness of the c-domains of the elementary regions of the ordered phase in a uniform crystal structure is a fraction of a micron (Fig. 1a,b), the width of the magnetic domains reaches several microns. This means that each magnetic domain is a macrodomain and encloses a large number of crystalline c-domains, differing in the orientation of the easy axis. This conclusion has been verified experimentally as shown in Fig. 5, which shows an electron microscope photograph of a portion of a domain structure of the "comb" type (Fig. 5a), of the leaf type (Fig. 5b), and the zigzag type (Fig. 5c), taken by means of magnetic replicas. The fine-powder suspension is observed within the structure of the plate and provides information on the mutual arrangement of the macrodomain walls and the boundaries of the c-domains on various cross sections of the stack of plates. Figure 5a shows that on the base of the stack the macrodomain walls of the main macrodomains are oriented along the traces of the boundaries of the c-domains (compare with Fig. 4e), and the boundaries of the c-domains intersect at the prismatic (Fig. 5c) and the pyramidal planes at a large angle (compare with Fig. 4c and 4d, respectively).

It has been noted above that magnetic domain walls of the Neél type are formed on the invariant boundaries of the c-domains. The crystalline c-domains are magnetic microdomains. As shown in our work,[16–20] the characteristic angle of the microdomain walls depends on the thickness of the c-domains and the constants of the material, but for a thickness $d \geqslant 0.02\ \mu$m we can say approximately that these are 90° walls. In this way, in a regular twinned system of plates of exchange-interacting uniaxial crystals the same intensity arises as in a multiaxis ferromagnet:[32,33] the existence of a net magnetic moment in a system of 90° microdomains results in the formation of a macrodomain magnetic structure with 180° Bloch walls within the c-domains. It follows from direct observation of the domain structure that the magnetically independent regions of the ordered phase are not the individual c-domains, but the plates and/or the stacks of poly-twinned plates that have grown from a single center of ordering. The magnetic domain structure is cooperative in nature. If a c-domain were an isolated region of ordered phase, the width of the magnetic domains, according to the theory of thin plate-like crystals, would be only a fraction of a micron.[34]

Figure 6 shows pictures of a cooperative magnetic domain structure on various crystallographic planes of single-crystal CoPt heated to 1000 °C and cooled from 850 to 750 °C over a period of six hours with subsequent quenching in water. After this treatment the crystal has a microstructure that is very nonuniform in size and internal structure and has poor hysteresis properties ($H_c = 160$ kA/m, $j_r = 0.3$; Ref. 35). In addition to the zigzag domain structure discussed above (Fig. 6a), the CoPt crystal shows new domain structure configurations not seen in FePt. For example, on the (010) cross section the macrodomains of magnetic walls are arranged along the boundaries of the poly-twinned plates (Fig. 6b), whereas in the corresponding stack of the FePt crystal the microdomain walls are inclined to the boundaries of the plates at an angle of $\approx \pi/4$ (Fig. 4d). On the (110) surface of the CoPt crystal the overall shape of a magnetic domain structure is reminiscent of a labyrinthine domain structure on the basal plane of a bulk uniaxial ferromagnet (Fig. 6c). Only with a detailed examination does one observe microscopic regions with a more or less regular domain structure that differ among themselves by the mean orientation of the macrodomain walls.

Comparing the microstructure of the domain structure

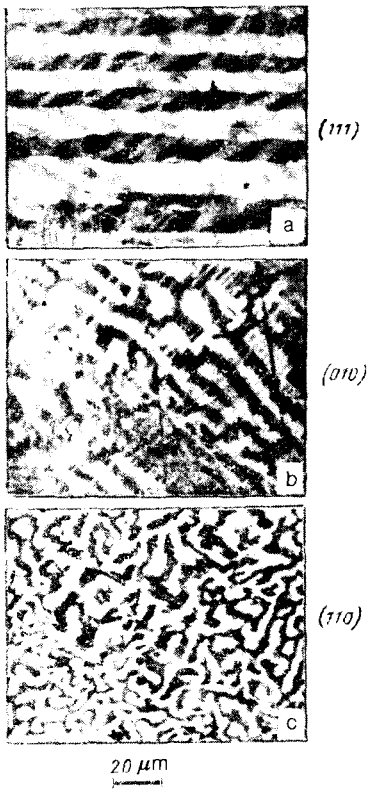

FIG. 6. Magnetic domain structure of a CoPt poly-twinned crystal after cooling from 850 to 750 °C over a period of 6 h and then annealing at 750 °C for 4 h. The domain structure is revealed by means of the polar Kerr effect on (a) the {111} planes; b) the {010} planes; c) the {110} planes.

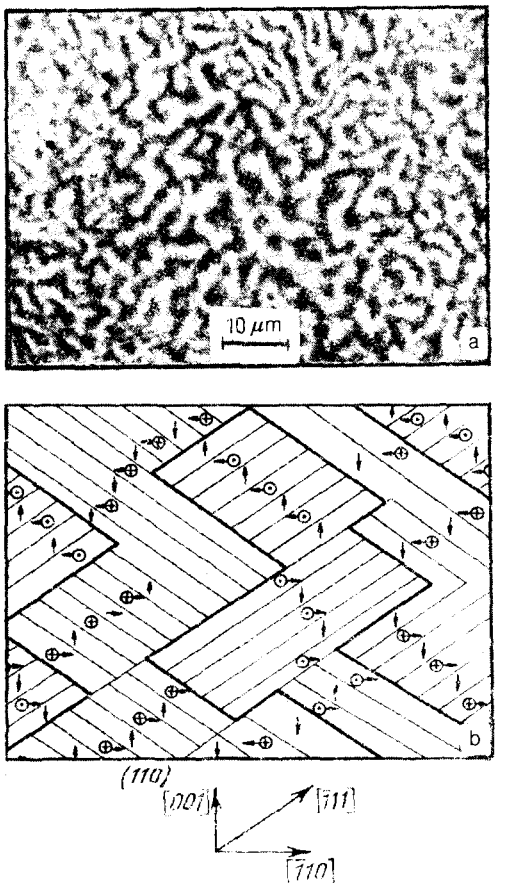

FIG. 7. Magnetic domain structure of a poly-twinned CoPt crystal after annealing at 660 °C for 30 min. a) Pattern as revealed by means of the polar Kerr effect; b) its interpretation on the (110) surface. The fine lines show the boundaries of the c-domains and the heavy lines show the boundaries of the macrodomain walls. Notation for the orientation of the magnetization vectors in the c-domains relative to the surface of observation: ↓ ↑ parallel; ⊙ ⊕ at an angle of $\pi/4$.

of FePt and CoPt crystals, one can conclude that the formation of new domain structure configurations is related to the change in the thickness of the c-domains and to the internal structure and the dimensions of the twinned systems, and, as a consequence, to the change in the crystallographic orientation of the 180° magnetic walls.

3.3. Domain structure of crystals with highly dispersed twinned microstructure

After the CoPt crystal has been quenched in water from 1000 °C and then thermally annealed at 660 °C for 20 to 60 min an ordered phase is formed in it that consists of highly dispersed blocks of c-domains. The most characteristic feature of this state of the ordered CoPt crystal is the irregular labyrinthine domain structure. The minimum size D of the magnetic domains is comparable to the ultimate resolution of an optical microscope. It is important to note that on the two mutually perpendicular (110) and (001) planes the domain structures can scarcely be distinguished by their shapes.[31] The pattern of the domain structure on a {110} surface is shown in Fig. 7a. A comparison of the domain structure with the microstructure of the CoPt (Figs. 1d and 7a) shows that the magnetic domains are not only considerably wider than the individual c-domains, but are also actually wider than the linear dimensions of the regular system of c-domains. Thus, a single magnetic domain encompasses several blocks of c-domains and is a macrodomain. A possible interpretation of the magnetic domains in the domain structure of the CoPt crystal in this case may be the scheme illustrated in Fig. 7b. Here it can be seen that the macrodomain walls, indicated by the system of heavy lines, are found only at the boundaries of the blocks of c-domains, unlike the domain structure of the FePt and CoPt crystals shown in Figs. 4–6, where the domain walls are located in the interior of the regular systems of c-domains.

Near the Curie temperature, natural sites for the formation of magnetic domain walls are the boundaries of the blocks of c-domains with internal stresses. As the temperature is lowered below the Curie temperature, $T < T_c$, the internal stresses hinder the redistribution of the domain walls to comply with the temperature variation of the saturation magnetization M_s and the magnetic anisotropy constant K. Therefore the domain structure in a thermally demagnetized CoPt crystal treated to produce the optimum hysteresis properties is not in a state of equilibrium.

Thus, there exist magnetic domains of various orders in poly-twinned FePt or CoPt crystals with different degrees of dispersion of the twinned systems and of the c-domains that form them. These are magnetic microdomains that coincide with crystalline c-domains and magnetic macrodomains that include a large number of c-domains. In other words, the hierarchy in the microstructure of ordered alloys (c-do-

mains, blocks, plates, stacks) formed in the *fcc–fct* phase transition also corresponds to the hierarchy in the magnetic domain structure. The cooperative phenomena, that is, the self-organization in the ferromagnetic twinned system, are due to the exchange and magnetostatic interactions at the twin boundaries of the *c*-domains.

4. MAGNETIC DOMAIN WALLS IN A POLY-TWINNED CRYSTAL

It is clear from the above discussion that a ferromagnetic poly-twinned crystal contains magnetic microdomain walls that coincide with the boundaries of the crystalline *c*-domains, as well as magnetic macrodomain walls that intersect a large number of *c*-domains. Let us examine the structural features of the two kinds of walls.

4.1. Microdomain walls

Microdomain magnetic walls that are pinned at twin boundaries are structurally similar to ordinary domain boundaries but at the same time they differ qualitatively from the latter in that they do not move in a magnetic field. Analytic expressions have been derived[15–18] for the energy of Bloch (B) and Neél (N) walls over the entire range of thickness of the *c*-domains. It was shown that in the CoPt, FePt, and FePd alloys the energetically more favorable walls are the "frozen-in" Neél (N-type) walls. For these walls we shall present only approximate expressions that are valid beginning with a relative *c*-domain thickness $\xi_0 = d/\delta_0 \geqslant 5 (\delta_0 = (A/K)^{1/2}$, the Landau–Lifshitz parameter that characterizes the width of a magnetic domain wall. Neél walls of two types, N_1 and N_2, have been analyzed in Refs. 15 and 16. In the domain walls of type N_1 the magnetic moment at the center of the twin boundary is directed along the normal to the plane of the boundary. The magnetostatic energy associated with the formation of this wall is small and its contribution to the total energy can be neglected.[20,35] In this approximation the surface density of the energy of a Neél wall is

$$\gamma_{N_1}^{2\alpha} = \gamma_B^{180}(1 - \cos\alpha); \tag{1}$$

where $\gamma_B^{180} = 4K\delta_0$ is the surface energy density of the 180° Bloch walls in a uniaxial crystal. For $\alpha = \pi/4$,

$$\gamma_{N_1}^{90} = 0.3\gamma_B^{180}. \tag{2}$$

If a Bloch magnetic transition layer is formed on the twin boundary of the *c*-domains, then the surface density of the energy will be

$$\gamma_B^{2\alpha} = \gamma_B^{180}\sin^2\alpha \times\left[2 - (1 - \cos^2\alpha)^{1/2} - 2\,\frac{\cos^2\alpha}{\sin\alpha}\ln\frac{\sin\alpha + (1 + \cos\alpha)^{1/2}}{\sqrt{2}(1 + \sin\alpha)}\right]. \tag{3}$$

For $\alpha = \pi/4$ we have

$$\gamma_B^{90} \approx 0.5\gamma_B^{180}. \tag{4}$$

Consequently, $\gamma_{N_1}^{90} < \gamma_B^{90}$, which confirms the existence of type N_1 Neél walls on the twin boundaries.

The characteristic feature of the structure of the walls of type N_2 is that in the center of the twin boundary the vector **M** lies in the plane of the wall. The surface energy density of these walls is

$$\gamma_{N_2}^{2\alpha} = \chi\gamma_B^{180}, \tag{5}$$

$$\chi = \left[a^{1/2} + \frac{(a+b)^{1/2}}{2}\right] + \frac{1}{8}\xi_0(1 - \eta - a); \tag{6}$$

$$a = (b^2 + \sin^2\alpha)^{1/2}, \quad b = \eta + \cos 2\alpha, \quad \eta = 2\pi M_s^2/K. \tag{7}$$

For a given angle of misorientation of the easy axis the energy of the Neél wall of type N_2 is determined by the magnetostatic interaction parameter η (Ref. 17) and is larger for larger η.

4.2. Macrodomain walls

Macrodomains are separated by 180° Bloch walls. From general considerations we can assume that the mean orientation and the total energy of a macrodomain wall in a stack of poly-twinned plates depends on the crystallographic orientation of its 180° sections within the *c*-domains and the magnetic structure of the regions where the 180° Bloch walls and the 90° Neél walls intersect.

Figure 8 shows schematically a diagram of possible configurations of macrodomain structure on the basal crystallographic planes of a stack of poly-twinned plates with a (110) base for the case where the 180° walls in the *c*-domains are arranged along the planes of type {100} (column A) or along the {110} planes (column B). It can be seen that on some planes the mean orientations of the macrodomain walls in the two cases can be close together or even coincide (e.g., the (001) plane in Figs. 8A and 8B). However, on the (110) basal plane and the (010) pyramidal planes the domain structures are quite different in the mean orientations of the macrodomain walls (compare Figs. 8Aa with 8Ba, and 8A d with 8B d).

Experiments have shown that domain structure configurations of type A are observed in those stacks of poly-twinned plates that consist of *c*-domains of various thicknesses $d > 1$ μm (Ref. 31). Poly-twinned plates with such domain structures were observed on the {110} and {010} surfaces of the CoPt crystal (compare, e.g., the diagram in Fig. 8A d with Fig. 6b). In the FePt crystal, where the thickness of the *c*-domains is $d \sim 0.1$ μm configurations of type A were not obtained. The domain-wall configurations that were best observed in FePt were those that correspond to the diagram in Fig. 8B. Therefore, the most probable planes of the 180° macrodomain magnetic walls in the FePt alloy are the {110}. One can make out types of macrodomain walls, which differ in their mean orientations relative to the junction plane of the poly-twinned plates (Fig. 8B, the (001) plane). The walls of the first type (*1*) consist of only 180° Bloch walls and regions of their intersection with 90° Neél walls, N_1. Macrodomain walls of type *2* include regions of charged 90° walls. It may be presumed that the magnetic structure of these regions is similar to the distribution of the magnetization in type N_2 Neél walls. The total area of the 180° B regions in macrodomain walls of type (*1*) is considerably larger than in the walls of type (*2*), but the walls of the former type do not contain charged Neél regions. A theoretical estimate for a particular case has been given[36] for the

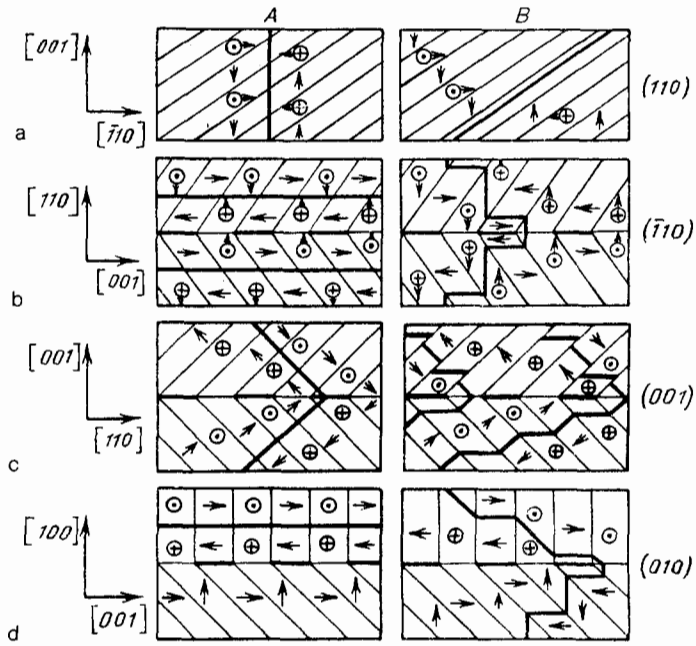

FIG. 8. Diagram of the possible configurations of the main macrodomains on some planes of a stack of poly-twinned plates. The base of the stack is taken to be the (110) plane. The fine lines show the boundaries of the c-domains, the heavy lines the 180° parts of the macrodomain magnetic walls. A) the planes of the 180° walls are the (100) and the (010) plane, alternating in adjacent plates. B) The planes of the 180° walls are the {110} planes.

relative critical thickness ξ_0 of the c-domains below which the existence of macrodomains walls of the second type is energetically unfavorable. For the FePt alloy this value is $\xi_0 = 170$, whereas for the FePd alloy, $\xi_0 = 49$, which correspond to 0.5 and 0.15 μm, respectively. The average thickness of the c-domains in FePt is close to 0.1 μm, that is, macrodomain walls of the second type are permitted theoretically. Unfortunately, this estimate was made without taking into account the energy of the region of intersection of the Bloch and Neél walls ($B - N$ intersection).

4.3. Intersection of micro- and macrodomain walls

The region of $B - N$ intersection can be regarded as a kind of analog of the well-known Bloch lines in the block domain walls of magnetic crystals. An exact calculation of the distribution of the magnetization in the region of $B - N$ intersection is beset with great mathematical difficulties. With a number of simplifying assumptions, the energy of a $B - N$ intersection has been estimated in Ref. 38. A diagram of intersecting 180° Bloch walls and 90° Neél walls and the distribution of the magnetization in the region of the $B - N$ intersection in the yz plane, used for the calculation are shown in Figs. 9 and 10, respectively.

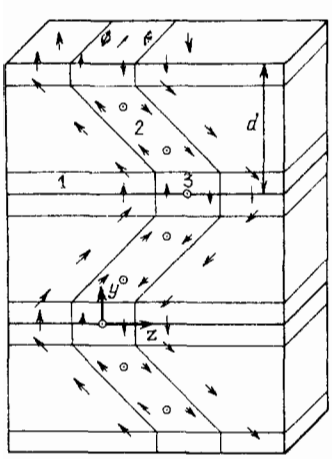

FIG. 9. Arrangement of magnetic domain walls in a poly-twinned crystal. *1*. Neél wall (N_1); pinned on a twinning boundary; *2*- 180° Bloch macrodomain wall (B); *3*- region of intersection (B–N) of Bloch and Neél walls. The x axis is perpendicular to the plane of the figure.

According to Ref. 38, the energy density per unit length in the region of the $B - N$ intersection is

$$\gamma_{B-N}^{2\alpha} = \pi\lambda_{B-N}^{2\alpha}\delta_\theta\gamma_\varphi, \tag{8}$$

where

$$\gamma_\varphi = 4K\delta_\varphi, \tag{9}$$

$$\lambda_{B-N}^{2\alpha} = \left[\frac{\alpha}{\sin\alpha}\tanh\frac{\pi}{2} + \left(\frac{\pi}{2} - \tanh\frac{\pi}{2}\right)\sin^2\alpha\,\frac{\tanh(\alpha/\sin\alpha)}{1+\cos\alpha\cdot\tanh(\alpha/\sin\alpha\lambda)}\right], \tag{10}$$

$$\delta_\varphi^2 = \frac{A_1\sin^2\alpha + A_2\cos^2\alpha}{2k}, \quad \delta_\theta = \frac{A_1\cos^2\alpha + A_2\sin^2\alpha}{2k}, \tag{11}$$

A_1 and A_2 are, respectively, the exchange interaction parameters along the tetragonal axis and in the basal plane of the crystal, and φ and θ are the azimuthal and polar angles that define the orientation of the magnetization vector in the region of the $B - N$ intersection. The angles φ and θ vary over the range $2\Delta_\varphi \cdot 2\Delta_\theta$ (see Fig. 10):

$$\Delta_\varphi = (\alpha/\sin\alpha)\delta_\varphi, \quad \Delta_\theta = (\pi/2)\delta_\theta. \tag{12}$$

For $2\alpha = \pi/2$ the energy γ_{B-N}^{90} is less than the energy density of a uniform 180° Bloch wall and amounts to $0.755\gamma_B^{180}$. It follows directly from the relation $\gamma_{B-N}^{90} < \gamma_B^{180}$

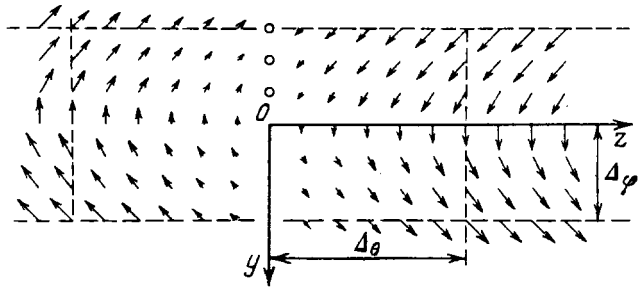

FIG. 10. Schematic diagram of the distribution of the projections of the magnetization vectors **M** on the *yz* plane in the region of intersection of Bloch and Neél walls.

that the larger is the number of twin boundaries a mobile macrodomain wall intersects the lower will be the total energy. From this result we have not only a new and previously unrecognized contribution to the magnetic hysteresis resulting from the hindered motion of domain walls at regions with the highest density of twin boundaries, but also find an explicit relation between the coercive force H_c and the parameters of the twinned microstructure.[39]

4.4. Microdomain walls in a magnetic field

Before proceeding to a discussion of the behavior of the domain structure during magnetization reversal in a twinned system, it is logical to analyze the change in the structure of microdomain walls in a magnetic field. Very little has heretofore been done along this line. The most complete study has been a theoretical treatment of the structure of microdomain walls pinned to twin boundaries.[16] We shall present some results that pertain to a single wall ($d \to \infty$) in a magnetic field perpendicular to the plane of the wall.

In a field parallel to the intrinsic magnetic moment of a wall of type N_1 (Fig. 11a, upper diagram) the "angle" of the wall (the angle θ in Fig. 11b) and the energy density (Fig. 11c) decrease with an increase in the quantity

$$h = \frac{H}{H_a} = \frac{H}{K/M_s}$$

In a negative field, on the other hand, both these quantities increase. In a field $h = -0.5$ the orientation of the magnetization **M** in the domains changes discontinuously. As a result, the distribution of the magnetization vectors **M** in the wall become complicated (the lower diagram in Fig. 11a). The vector **M** rotates by $360° + 2\theta$ in going through the twin boundary. The energy of the wall increases severalfold and continues to increase with increasing $|-h|$. The opposite result is obtained for a Bloch wall.

Figure 11c shows plots of $(\gamma_{N_1}/\gamma_0)(h)$ for various values of the parameter $\eta = 2\pi M_s^2/K$ (the solid lines) and a plot of $(\gamma_B/\gamma_0)(h)$, the dashed line. It can be seen that the energy of a Bloch wall in negative fields can be less than the energy of an N_1 Neél wall. That means that the magnetic field can cause a change in the type of microdomain wall.

The distribution of the magnetization in a microdomain wall thus changes in a magnetic field, along with the effective width and the energy density: these changes can be discontinuous and result in complicated distributions of the magnetization of the wall. Finally, for certain conditions changes in the type of microdomain can be expected under the action of a magnetic field. The effect of a magnetic field on the structure of 180° Bloch macrodomain walls should in the first approximation be the same as for homogeneous 180° Bloch walls.[40] We did not study the change in the structure and energy of $B - N$ intersection lines in a magnetic field.

5. CHANGE IN COOPERATIVE DOMAIN STRUCTURE IN A MAGNETIC FIELD

The forms of behavior of the changes in the domain structure in a magnetic field for a single stack of poly-twinned plates have been established in a study of the domain structure in cross sections of stacks with different orientations relative to the (110) and (001) observation surfaces of plate samples of FePt. The field H makes an angle ψ with the normal to the base of the stack or an angle φ with the [100] direction if it lies in the basal plane of the stack (Fig. 12).[41]

5.1. Magnetization of a stack of poly-twinned plates

During magnetization, macrodomain walls move and the macrodomains disappear. The shape of the walls and the nature of their motion depend strongly on the magnitude

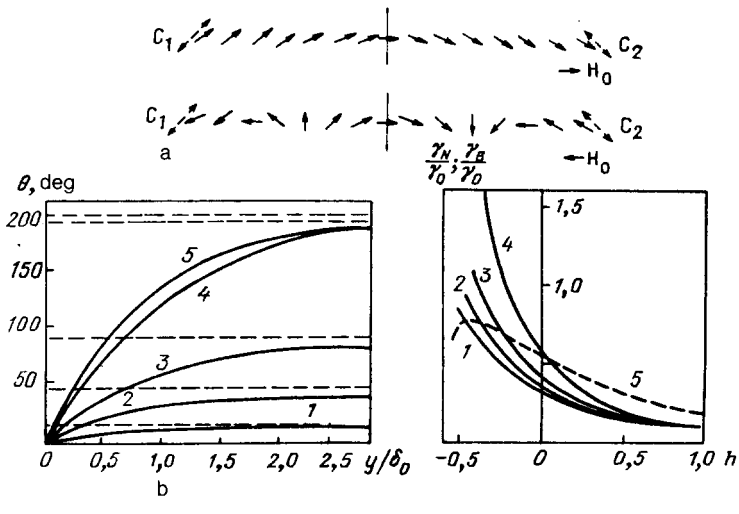

FIG. 11. Behavior of microdomain walls in a magnetic field. a) Schematic distribution of the **M** vectors in a Neél microdomain wall; upper and lower diagrams, respectively: before and after the discontinuous change in the magnetization in a reverse magnetic field. b) Dependence of the polar angle θ in the Neél microdomain wall (N_1) on the reduced coordinate y/δ_0 for various reduced magnetic fields h differing in magnitude and sign: *1*) $h = 2.0$; *2*) $h = 0$; *3*) $h = -0.5$; *4*) $h = -1.0$, and *5*) $h = -2.0$ for the case $\alpha = 45°$ and $\eta = 1$. c) Dependence of Bloch wall energy (dashed line) and Neél wall energy (solid lines) on the field h: *1*) $h = 0.5$; *2*) $h = 1.0$; *3*) $h = 3.0$; *4*) $h = 10$ for $\alpha = 45°$ and $\eta = 1$.

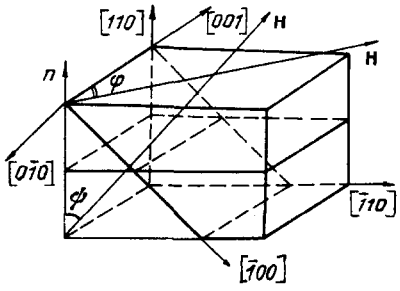

FIG. 12. Distribution of stacks of poly-twinned plates with a (110) junction plane and the orientation of the external magnetic field **H** relative to the crystallographic directions of the initial disordered single crystal. The quantity ψ is the angle between the direction of **H** and the normal to the base of the stack; φ is the angle between the direction of **H** and the [001] axis in the basal plane of the stack.

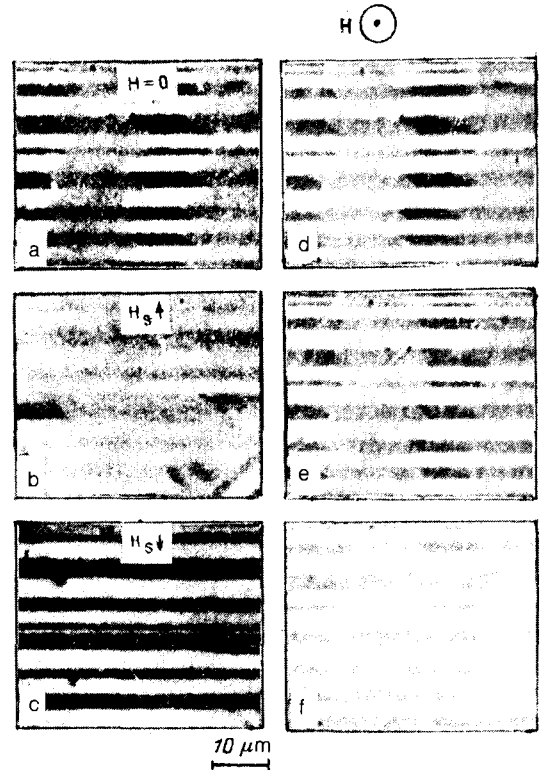

FIG. 13. Variation of the magnetic domain structure on the (001) surface of a stack of poly-twinned plates during magnetization of FePt crystal. b,c) The field **H** points along the normal to the base of the stack or, d–f) parallel to the plane of the base of the stack and is equal to: a) 0; b) $H_s = 200$ kA/m; c) H_s; d) 280 kA/m; e) 416 kA/m; f) 528 kA/m.

and orientation of the external magnetic field. If the magnetic field **H** is along the normal to the base of the stack ($\psi = 0$), then zigzag macrodomain walls move parallel to themselves as an entire unit, and it is easy for them to slide along the boundaries of the poly-twinned plates practically without hindrance. The magnetization is already complete in fields $H_s \approx 200$ kA/m (Fig. 13b,c), where H_s is the field at which the macrodomain magnetic structure disappears. A diagram of the variation in the domain structure for $\psi = 0$ is shown in Fig. 14a–c. After magnetization, the (100) surface of the stacks of poly-twinned plates has the color of those zigzag microdomains (gray or black-white; see Figs. 13a and 14a) in which the orientation of the net magnetization coincides with the direction of the applied field. For instance, in a field $\mathbf{H}_s$ directed along the upward normal to the base of the stack, adjacent planes are practically indistinguishable in contrast (Fig. 13b) while in a field $\mathbf{H}_s$ of the opposite sign (Figs. 13c and 14c) the contrast is maximum.

The angle between the normal to the base of the stack and the direction of the external magnetic field can be varied by rotating the sample about the optical axis of the microscope. Although the change in the orientation of the plane of polarization relative to the crystallographic directions of the sample causes a change in the contrast between macrodomains, the nature of the motion of the macrodomain walls discussed above stays the same over the entire range of angles $0 < \psi < \pi/4$.

If the magnetic field is applied at an angle $\pi/4 < \psi < 3\pi/4$ or in the basal plane of the stack, the behavior of the domain structure is more complicated. If the field

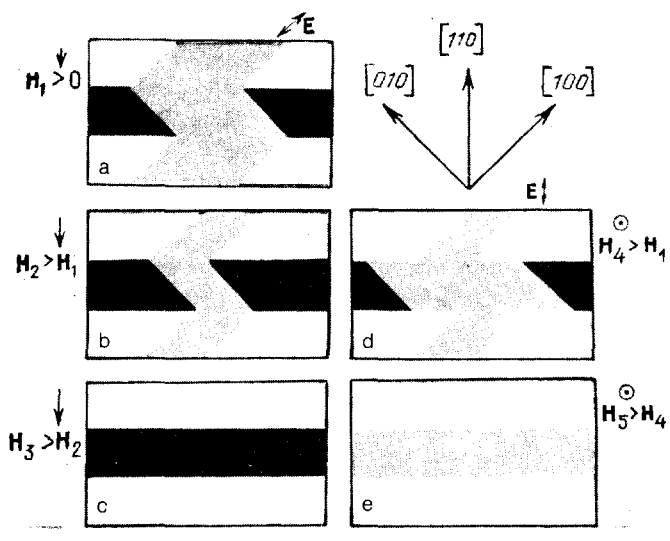

FIG. 14. Variation in the domain structure on the (001) surface of a stack of poly-twinned plates of an FePt crystal in magnetic fields of various orientations. a,b) **H** perpendicular to the base of the stack ($\psi = 0$); c,d) **H** parallel to the base of the stack ($\varphi = 0$).

is perpendicular to the (001) surface of observation, i.e., if it lies in the basal plane of the stack ($\varphi = 0$), the volume of these microdomains or their fragments whose component of magnetization is parallel to the field **H** will increase and the volume of the fragments with a magnetization component antiparallel to the magnetic field will decrease. In agreement with the interpretation of the domain structure (see. e.g., Fig. 8*B*c), the portions of the same macrodomain wall in adjacent plates must move in different directions. A diagram of the proposed change in the domain structure is shown in Fig. 14d,e. As judged from the picture of a real domain structure (Fig. 13d–f) this actually happens, but the motion of domain walls in that experimental geometry is strongly hindered. Up to fields $H = 80$ kA/m large changes in the domain structure do not occur (Fig. 13a), and then the walls of the white fragments begin to move, undergoing considerable bending within the poly-twinned plates (Fig. 13d,e). Strong pinning at the macrodomain walls is observed on the boundaries of the plates. The walls of the black fragments scarcely move at all. In fields $H = 400$ kA/m the motion of the white fragments stops and further magnetization reversal comes about through the formation of regions magnetized in the direction of the field within the domains magnetized opposite to the field [the gray fragments within the black and the white fragments within the gray (Fig. 13e)]. As a result, the pattern of zigzag macrodomains (Fig. 13a) is converted to a pattern of white and gray stripes (or gray and black stripes; Fig. 13f). As judged from the contrast in polarized light, the magnetization is completed in fields of 700–800 kA/m. It is still possible, however, that residues of macrodomains remain in the boundaries of the plates also in higher fields.

According to theory,[42] the hindrance of the motion of a domain wall is the greatest if the plane of the defect and the domain wall coincide. This conclusion also applies to the macrodomain walls located at the boundaries of poly-twinned plates (Fig. 8*B*). However, experiments have shown that the motion of macrodomain walls inclined to the boundaries of the plates is also hindered. The observed retardation in the motion of macrodomain walls is evidently related to the interaction of mobile 180° Bloch walls with 90° Neél walls frozen at the twin boundaries.

5.2. The two types of microdomain structure

It appears from observations of domain structure that a quasisaturated state is achieved in fields $H > H_s$—the macrodomain walls within a poly-twinned plate disappear and the plate becomes a macro-single-domain macrodomain plate (Figs. 13b,c and 14c,e). However, the microdomain structure can exist up to fields comparable with the anisotropy field H_a. Microdomains are not resolved in an optical microscope, since the thickness of the *c*-domains is ~ 0.1 μm. An analysis of the contrast pattern on the same cross section of the stacks of plates for various directions of the external magnetic field $H \geqslant H_s$ allows us to interpret the microdomain magnetic structure of the plates. It is assumed that the contrast on a poly-twinned plate is a simple superposition of the contrasts from the individual *c*-domains that make up the plate (see Sec. 3.1). It is also assumed that the magnetization vectors deviate very little from the easy axis in the center of thick *c*-domains ($d \approx 0.1$ μm) as a result of the exchange interaction[16–21] or in a magnetic field $H = 0.1$

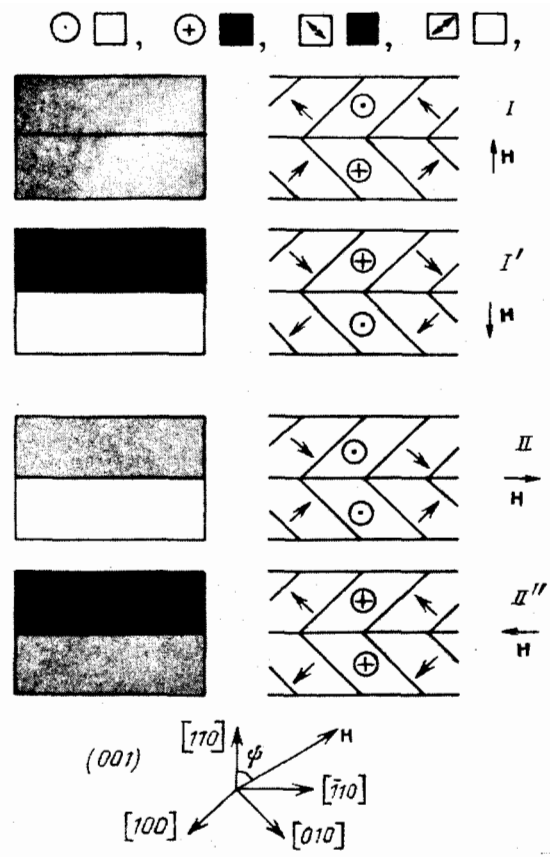

FIG. 15. Interpretation of the microdomain structure on the (001) surface of a poly-twinned FePt crystal for various orientations of the external field $\mathbf{H} > \mathbf{H}_s$ relative to the base (110) of the stack. a,b) **H** perpendicular to the base of the stack ($\psi = 0$); c,d) **H** parallel to the base of the stack ($\psi = 90°$).

H_a (Refs. 2–4). This deviation was not taken into account in analyzing the patterns.

For various directions of the external field, stable (I,I′) and metastable (II,II′) quasisaturated states, differing in their microdomain structure (Fig. 15a–e), are formed. The state I(I′) is formed when a stack is magnetized in the range of angles $0 < \psi < \pi/4$ and is characterized by the absence of magnetic charge and the formation of N_1 microdomain walls at the twin boundaries of the *c*-domains (Fig. 15a,b). The state II (II′) is obtained for magnetization in the range $\pi/4 < \psi < \pi/2$ (Fig. 15c,d). In this case magnetic charge is formed at the boundaries of the poly-twinned plates and charged Neél walls, of type N_2, are formed. The existence of analogous magnetic states was predicted theoretically in a calculation of the process of magnetization reversal of twinned systems in a model of uniform rotation of the magnetization vectors with allowance for the magnetostatic interaction.[20,22–24]

5.3. Magnetization reversal of a stack of poly-twinned plates. The two types of macrodomain magnetic structures

The magnetization reversal of a stack of poly-twinned plates consists of a transition from one single macrodomain structure to the other (I ⇄ I′, II ⇄ II′) and occurs by the formation and growth of macrodomains.

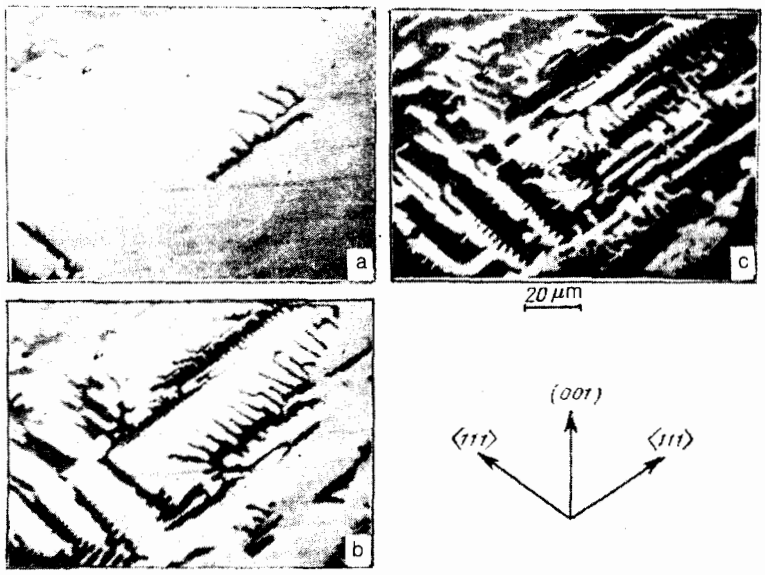

FIG. 16. Variation in the domain structure on the (110) basal plane of a stack of poly-twinned plates during magnetization reversal of an FePt crystal. The domain structure is revealed by means of the polar Kerr effect. The magnetic field **H** is perpendicular to the basal plane and equal to: a) 208; b) 64; and c) 80 kA/m.

5.3.1. Domain structure of poly-twinned plates in a magnetic field perpendicular to the base of the stack

Figure 16 shows the pattern of changes of the domain structure on the (110) basal plane of a stack of poly-twinned plates of a FePt crystal in a magnetic field H perpendicular to this surface ($\psi = 0$). As a rule, the main domains are formed abruptly at locations where poly-twinned plates abut, and they appear as stripes oriented along the different ⟨111⟩ directions (Fig. 16a). The larger these centers of formation of the domain structure are—that is, the smaller are the stacks with a regular microstructure—the less regular the domain structure becomes, since the domain walls very frequently are located along the boundaries of the stacks. As the magnetic field is further reduced, new macrodomains are formed (Fig. 16b) and the macrodomains move (Fig. 16c).

For the same magnetic field orientation $\mathbf{H} \| [110]$ it is possible to observe on the (001) plane perpendicular to the (110) plane the formation of zigzag macrodomains going through the entire stack of plates. The shape of these macrodomains and their subsequent behavior in a magnetic field is wholly similar to that described in Sec. 5.1 and in Figs. 13a–c and 14a–c. In the stacks having, e.g., a gray color (Fig. 13b) gray-white macrodomains appear abruptly (Fig. 13a) with walls that then move very rapidly in the magnetic field. The coercive force is mainly determined by the field at which the macrodomains appear, and, as determined from the domain structure patterns, is 25–40 kA/m.

It is important to emphasize that the polar Kerr effect reveals the changes in the magnetization only for those c-domains in which the vector **M** has a large component normal to the surface of observation.[29] Thus, observation of domain structure in two mutually perpendicular planes, the (110) and the (001) in combination, is evidence that for the same orientation of the external field relative to the base of the stack ($\mathbf{H} \| [110]$) irreversible changes in the magnetization occur simultaneously in all three types of c-domains that form the stacks of poly-twinned plates and that have mutually perpendicular easy axes (Fig. 8B). This confirms our conclusion that the individual c-domains are not magnetically saturated regions of ordered phase. Such regions are the poly-twinned plates and/or stacks of plates.

This kind of behavior in the changes in the domain structure during the magnetization reversal also holds for those cross sections of stacks of plates where the condition $0 < \psi < \pi/4$ is satisfied. Here it must be again emphasized that the preferred sites of formation of the macrodomains are the regions where the stacks abut and the boundaries of the poly-twinned plates.

The magnetization reversal of stacks of poly-twinned plates in the range of angles $0 < \psi < \pi/4$, that is, the transition $\mathrm{I} \rightleftarrows \mathrm{I}'$, thus proceeds by the discontinuous formation and growth of zigzag macrodomains. We shall designate the macrodomain structure that is formed in the $\mathrm{I} \rightleftarrows \mathrm{I}'$ transition as the DS_{I} structure. With a precision up to hysteresis effects, this structure is analogous to that of the domain structure observed in the thermally demagnetized state (Fig. 4).

5.3.2. Domain structure of stacks of poly-twinned plates in a magnetic field parallel to the base of the stack

For this orientation of the magnetic field ($H \| (110)$ and for the range of angles $\pi/4 < \psi \leqslant \pi/2$ the magnetization reversal occurs via the formation of two types of macrodomains of magnetic structure, $\mathrm{DS}_{\mathrm{I}(\mathrm{I}')}$ and $\mathrm{DS}_{\mathrm{II}(\mathrm{II}')}$, corresponding to the two types of microdomains of the magnetic states I and II. We shall present some examples without, however, going into a detailed description or an analysis of the $\mathrm{DS}_{\mathrm{II}}$ macrodomain structure.

Figure 17 shows the variations in the domain structure on the prismatic (110) cross section that result from the magnetization reversal of a stack along the [110] direction ($\psi = \varphi = \pi/2$). For this orientation of the external field **H** the adjacent poly-twinned plates cannot be distinguished by their contrast in polarized light. As the field **H** decreases, narrow inclined macrodomain walls grow out of the poly-twinned plates (Fig. 17a) and a more complicated "leaf" structure is formed. Within the individual plates the leafs

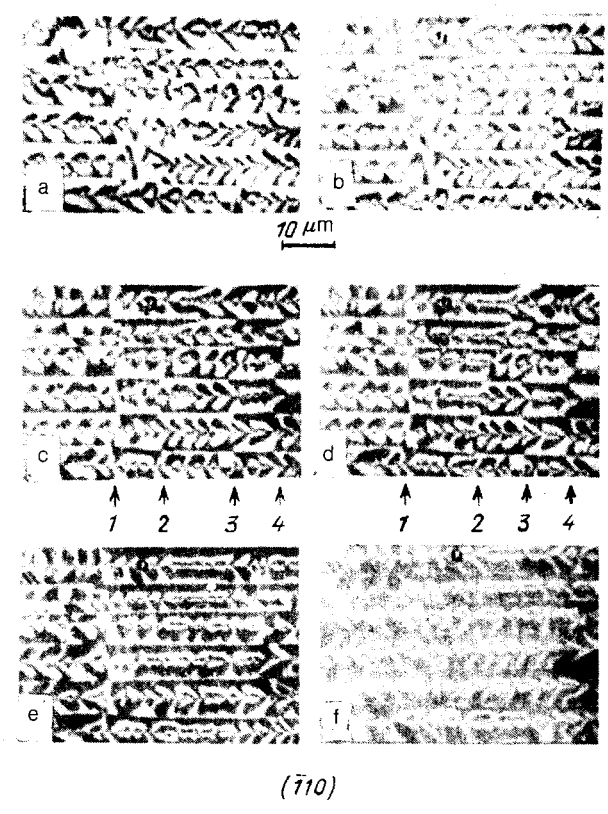

FIG. 17. Variation in the magnetic domain structure on the prismatic (110) plane of a stack of poly-twinned plates during magnetization reversal of an FePt crystal. The domain structure is revealed by means of the polar Kerr effect. The magnetic field **H** is perpendicular to the surface of observation ($\psi = \varphi = \pi/2$) and equal to a) 240; b) 88; c) -24;, d) -144; e) -200, and f) -332 kA/m. The arrows indicate the locations of the macrodomain walls *1*, *2*, *3*, and *4*.

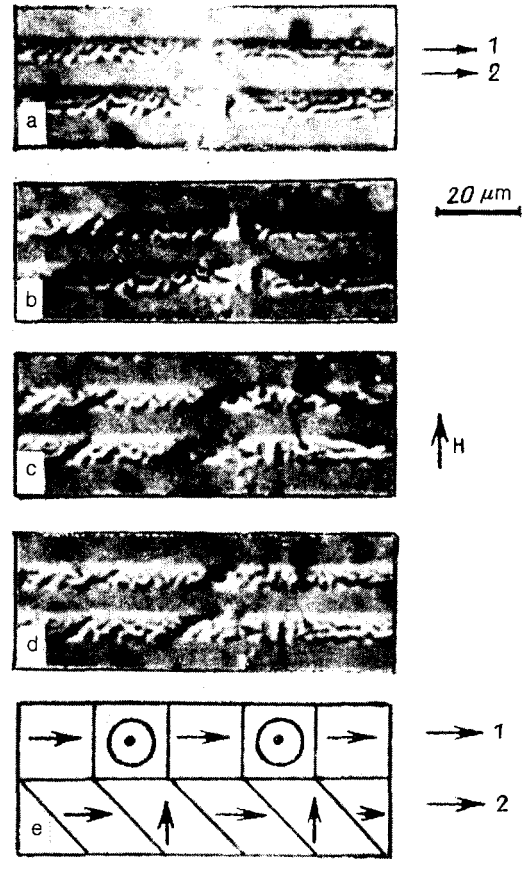

FIG. 18. Variation of the domain structure on the pyramidal (010) plane of a stack of poly-twinned plates during magnetization reversal of an FePt crystal. The domain structure is revealed by means of the polar Kerr effect. The magnetic field is applied in the (010) plane perpendicular to the boundaries of the plates and makes an angle $\psi \approx 45°$ to the [110] normal and is equal to: a) 4; b) -24; c) -72; and d) -112 kA/m. The lower diagram is that of the microstructure of plates *1* and *2*.

have the same color (Fig. 17b). As the magnetic field **H** is further reduced the motion of the DS_{II} macrodomain walls is hindered. In small negative fields broad zigzag macrodomain walls are abruptly formed (Fig. 17c). In each plate they can be distinguished by the different color of the additional domains: in the dark main domains the leafs are bright and in the bright main domains the leafs are dark. As the reverse magnetic field is increased further, some movement of the macrodomain walls of type DS_I is observed (compare Figs. 17c and 17d,e). After the disappearance of the DS_I structure the type DS_{II} structure is visible (Fig. 17f), and the latter also begins to disappear in fields $H > 300$ kA/m. contracting onto the boundaries of the plates.

Figure 18a–d shows diagrams of the domain structure observed on the (010) surface inclined to the base, with variation of the magnetic field applied in the (010) plane at an angle $\psi \approx \pi/4$. A diagram of the microstructure on this surface is shown in the lower part of the figure. After the sample is magnetized and the field is turned off macrodomains of type DS_{II} in a complicated configuration are visible on plate *1* (Fig. 18a). No domain structure is revealed at all on plate *2*, since the easy axis in the two types of *c*-domains that form the plate lie in the plane of observation. In a small negative field a white macrodomain DS_I appears abruptly (Fig. 18b) and as the field is further increased it moves along the boundary of the poly-twinned plate (Fig. 18c,d). This process ceases in fields $H \approx 200$ kA/m. With this experimental geometry domain structures of both types coexist in fields from 0 to 200 kA/m. The transition $DS_{II} \rightleftarrows DS_{II'}$ occurs only during the formation and motion of DS_I domains. The macrodomain structures DS_I and DS_{II} differ in their configuration, the width of the macrodomains, the range of angle and fields in which they exist, and their behavior in a magnetic field.

The general character of the variation of the domain structure in the range of angles $\pi/4 < \psi < \pi/2$ and the interpretation of the domain structure on the (001) plane are shown schematically in Fig. 19. In the maximum magnetic field a system of black and gray (or gray and white) stripes is seen; these are the poly-twinned plates (Fig. 19a). This pattern corresponds to the microdomain structure of type II (Fig. 15c). As the magnetic field is reduced a system of narrow inclined macrodomains of type DS_{II} are formed in every other plate (Fig. 19b). These DS_{II} domains arise out of the boundaries of the poly-twinned plates in order to reduce the magnetostatic energy of the magnetic charges that exist on the boundaries of the plates with domain structure of type II. As the magnetic field is further reduced, the DS_{II} walls no longer move, and further magnetization reversal occurs via the sudden formation of a zigzag DS_I structure at the loca-

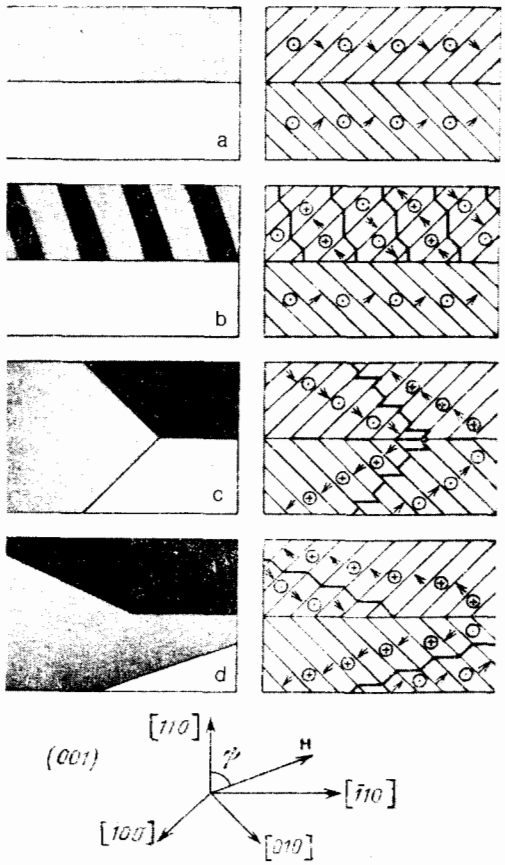

FIG. 19. Variation and interpretation of the magnetic domain structure on the (001) plane of a stack of poly-twinned plates during magnetization reversal of an FePt crystal. The magnetic field is applied perpendicularly to the (001) plane at an angle $\psi = 70°$ ($\pi/4 \leqslant \psi < \pi/2$).

tion of the DS_{II} structure and a gray and black-white zigzag macrodomain contrast, typical of this type of domain structure, appears and proceeds through the entire stack of plates (Fig. 19c). This pattern corresponds to the microdomain structure of type I with uncharged poly-twinned plate boundaries (Fig. 15a,b). In a certain field adjacent regions of the same macrodomain wall in mixed poly-twinned plates move in opposite directions (Fig. 19d). However the complete magnetization reversal of the stack via the motion of macrodomain walls of type DS_I is hindered. As the field is increased macrodomains of type DS_{II} are formed. In the maximum negative field, $H_m \geqslant H_s$, a pattern of black and gray stripes with microdomain structure of type II are formed (Fig. 15d). We note that in the states of type II (Fig. 19a) the resultant magnetization vector lies in the junction plane of the poly-twinned plates, while in the states I (I′) it points along the normal to the base of the stack (Fig. 19c).

The transition from state II to state II′ thus occurs not directly by the growth of macrodomains of type DS_{II}, but through the formation of "transverse" DS_I macrodomains, a process characteristic of the magnetization reversal process of multiaxial ferromagnets.[43] The coercive force in this case is also determined by the fields at which the DS_I macrodomains appear. This result is in qualitative agreement with the conclusions of the theory of Refs. 22–24.

5.4. Magnetization reversal of crystals with highly dispersed twin microstructure

When the nature of the contact changes and the conditions for closure of the magnetic flux at the boundaries of the poly-twinned plates are violated separate poly-twinned plates can become magnetically independent regions of ordered phase, and blocks of *c*-domains can do so if the regular ordered structure of the plates is disrupted. Here, changes are to be expected in the configuration and behavior of the domain structure during magnetization reversal and in the magnitude of the magnetic hysteresis characteristics.

Actually, in the magnetization reversal of CoPt crystals with a highly dispersed twinned microstructure, the reversed magnetic phase is formed in exceedingly high negative magnetic fields. The domains of the reverse-magnetization form discontinuously in individual microregions of the surface of a poly-twinned crystal as short lines or longer lines, situated along certain crystallographic directions. The regions of magnetization reversal are similar in size to the blocks of *c*-domains or groups of them (Fig. 20a,b), and the directions along which they form are the traces of the boundaries of regular twinned systems. Thus, the boundaries of the blocks of the *c*-domains or their groups act as grain boundaries, as do the boundaries of the stacks of poly-twinned plates.

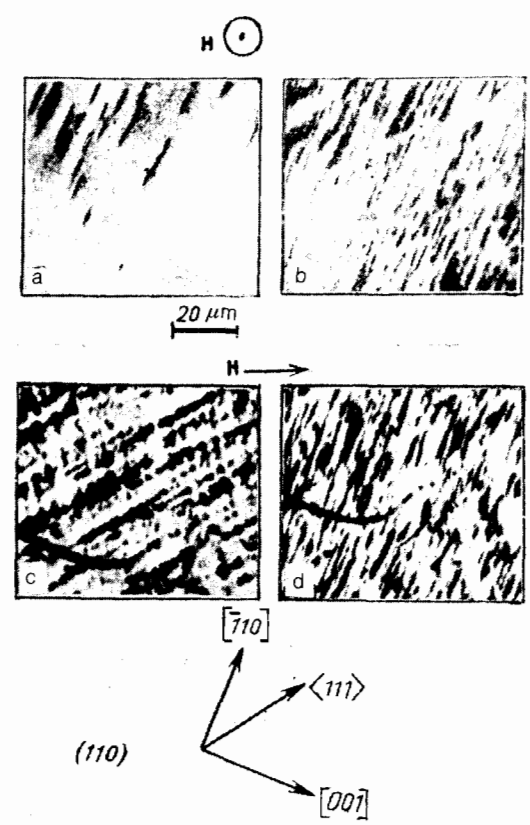

FIG. 20. Variation of the magnetic domain structure of a poly-twinned CoPt crystal after annealing at 660 °C for 30 min (the state with the optimum hysteresis properties) on the (110) surface in a magnetic field. a,b) Field **H** perpendicular to the surface of observation and equal, respectively, to -225 and -400 kA/m. The domain structure is revealed by means of the polar Kerr effect. c,d) **H** parallel to the (110) plane and equal, respectively, to -144 and -744 kA/m. The domain structure is revealed by means of a magnetic suspension.

Observations of domain structure during magnetization reversal of a CoPt crystal in a field parallel to the (110) plane have shown that domains of various orientations, ⟨001⟩, ⟨110⟩, and ⟨111⟩, can appear at the same location of a sample (Fig. 20c,d). It should be emphasized that for the same microstructure, ⟨110⟩ domains are observed by means of the polar Kerr effect (Fig. 20b), while the ⟨111⟩ domains (Fig. 20c) do not show up with this method, or have a very low contrast. We therefore suppose that the ⟨110⟩ and ⟨111⟩ domains differ in the ratio of the normal to the tangential component of the magnetization: in the ⟨110⟩ domains the vector **M** is inclined away from the *c* axes towards the [110] normal and in the ⟨111⟩ domains it is inclined towards the (110) planes. The reason for the inclination of **M** may be the exchange interaction, which operates on the twin boundaries of the *c*-domains.[16-21] On the basis of these results we conclude that in crystals with a highly dispersed twinned microstructure the magnetic states I(I′) and II(II′) also occur, similar to those that we predicted theoretically and observed in studies of magnetization reversal of a FePt crystal consisting of large stacks of poly-twinned plates.[41]

6. QUANTITATIVE RELATION BETWEEN THE PARAMETERS OF THE DOMAIN STRUCTURE AND THE CHARACTERISTIC DIMENSIONS OF THE ELEMENTS OF THE TWINNED MICROSTRUCTURE

6.1. Models of domain structure and the dependence of the domain width on the size of the stacks of poly-twinned plates

Studies of the form of magnetic domain structure and the behavior of the domain structure in a magnetic field show that the magnetically independent regions of ordered phase are not the individual magnetically uniaxial crystalline *c*-domains, but regular systems of *c*-domains (blocks, plates, stacks). The exchange and magnetostatic interactions at the twin boundaries result in an increase in the effective size of the magnetically independent regions. The boundaries of the regular systems of *c*-domains, on the other hand, play the role of grain boundaries. We can therefore assume that the width of the magnetic macrodomains depends primarily on the size of the stack of plates. In Ref. 36 we advanced two models of the magnetic domain structure of stacks of poly-twinned plates with a regular internal structure. These models are illustrated in Fig. 21 and they differ in their mean orientation, total area, and internal structure of the macrodomain walls. If we denote the projection of a *c*-domain on the *z* axis by *d*, then the dimensions of the poly-twinned plates L_1 and of the stacks L along the *z* axis will be, respectively,

$$L_1 = md + \Delta L_1, \quad 0 < \Delta L_1 \le d, \quad m = 0, 1, 2...,$$
$$L = 2kL_1, \quad k = 1, 2, 3..., \tag{13}$$

where k is the number of pairs of twinned plates in a stack. The period of the domain structure is $D = 2n(2d/\sqrt{3})$, where $2n$ is the number of *c*-domains in a half-period D. The displacement of the trace of a *c*-domain from the trace of a twin boundary on the surface of a stack is denoted by Δy (Fig. 21a). Let us also introduce the notation

$$l = m + \Delta l, \quad \Delta l = \Delta L_1/d, \quad 0 < \Delta l < 1,$$
$$\tau = (\sqrt{3}/2)\Delta y/d. \tag{14}$$

A numerical calculation of the relation between the width D of the macrodomains, the thickness d of the *c*-domains, and the dimension of a plate, L, for fixed values of L and d, respectively, is given for model (1). In the volume energy density f of the stack of plates we include the magnetostatic energy f_m and the energy of the magnetic domain walls, f_γ, of the Bloch and Neél domain walls. The energy of the regions of intersection of the Bloch and Neél walls is neglected in the calculation.

In the calculation of the intrinsic magnetostatic energy of the surface magnetic charges we assumed that the dimensions of a stack are infinite in the *xy* plane, the poly-twinned plates with regularly alternating easy axes are formed pairwise, and the plates all have the same thickness L_1. Then the magnetic charges that are formed on the upper and lower surfaces bounded by a stack of plates will be located one on top of the other. In this case, the volume magnetostatic energy density of these charges can be represented by the relations given in Ref. 44, and one can show that for the distribution $M_z(y) = (\sqrt{2}/2)M_y$, shown in Fig. 21a, a minimum

$$f_m = K\frac{2\eta n}{(3\pi^2 kl)^{1/2}}\sum\frac{1}{p^3}\frac{1-\exp(-\sqrt{3}\pi pkl/2n)}{\cos^2(\pi p/4n)}$$
$$\times\left[1 - 8\cos\frac{\pi p}{4n}\sin\frac{\pi p\tau}{4n}\sin\left[\frac{\pi p}{4n}(1-\tau)\right]\right]\Bigg\} \tag{15}$$

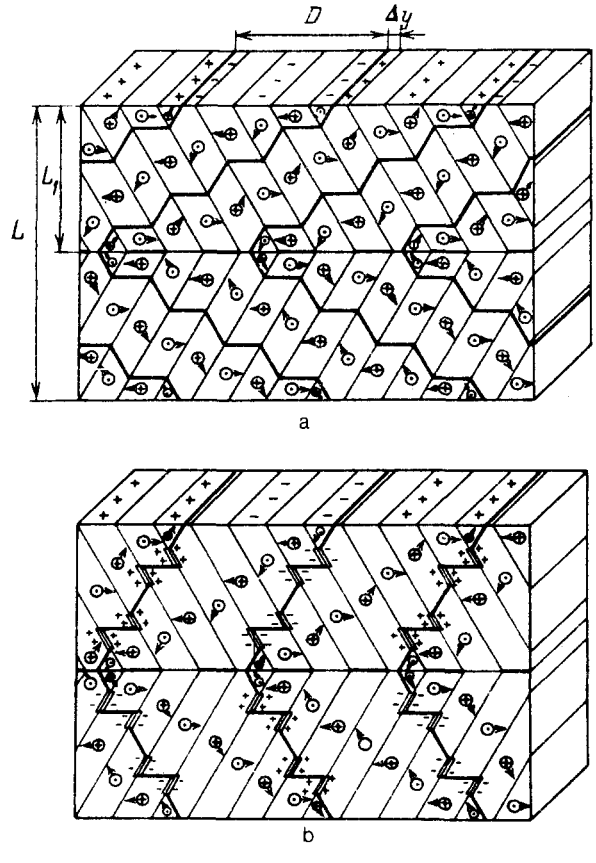

FIG. 21. Models of the magnetic domain structure of a stack consisting of two poly-twinned plates: a) without charged domain walls, and b) with charged domain walls.

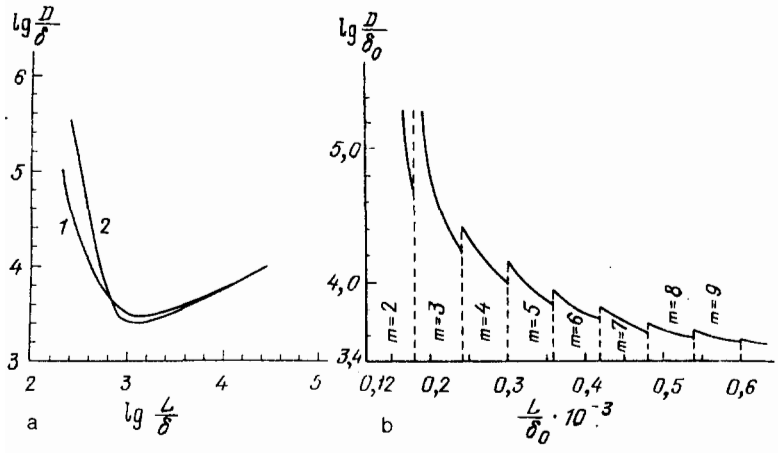

FIG. 22. Reduced width of macrodomains as a function of the reduced dimension of a stack of poly-twinned plates; a) for the case $L_1 = md$ (relative thickness of the c-domains $\xi_0 = d/\delta_0 = 30$ (curve *1*) and 200 (curve *2*), and b) for the case $L_1 = md + \Delta L_1$ (relative thickness of the c-domains $\xi_0 = 30$).

exists at the value $\tau = 0.5$. Here K is the anisotropy constant and η is the magnetostatic interaction parameter. In addition to the notation defined above [see formulas (13) and (14)] we also used the notation in Ref. 44.

The energy of all the domain walls, normalized to a unit volume of the crystal, is for model (1)

$$f_\gamma^{(1)} = \frac{4K}{\xi_0}\left[\frac{1}{n} + \frac{1}{2l}\left(\frac{\nu}{n} + \frac{2k-1}{2k} + 0{,}3\frac{2k-1}{4kl} + 1\right)\right], \quad (16)$$

where

$$\nu = \begin{cases} m & \text{for } 0 < \tau < \tau_{cr}, \\ m+1 & \text{for } \tau_{cr} < \tau < 1, \quad \tau_{cr} = 1 - \Delta l, \\ m & \text{for } \tau = 1. \end{cases} \quad (17)$$

The rest of the notation is defined above. For given material constants K and η, the energy $f = f_m + f_\gamma$ must take on a minimum value in terms of the discrete values n, the number of c-domains in a macrodomain of width D, and the continuous parameter τ, which is the displacement of a macrodomain wall relative the the c-domain boundary (Fig. 21a) The minimum energy is found with the use of a computer.

The general nature of the relation between the equilibrium width D of a macrodomain and the dimension L of a stack of plates is described by a Malek-Kambersky type of curve obtained for a uniform uniaxial crystal:[34] with increasing L there is at first a decrease and then an increase in the width of the macrodomains (Fig. 22a). In the range of dimensions $L > 10^4\delta_0$ (where $\delta_0 = (A/K)^{1/2}$), the curves of $D(L)$ for various values of $\xi_0 = d/\delta_0$ coincide, that is, they do not depend on the thickness of the c-domains that form the plate. If L_1, the thickness of the poly-twinned plate, is not an integer d ($L_1 = md + \Delta L_1$), the curves of $D(L)$, unlike those for a uniform crystal, exhibit discontinuous changes in the equilibrium thickness of the microdomains as the dimension L of a stack varies (Fig. 22b). This in turn, as is shown in Fig. 22b, leads to a situation where the dependence of the width of the macrodomains on the thickness of the stacks of poly-twinned plates is not single-valued. Even more conspicuous is the discontinuous and non-single-valued variation of the parameter D with a decrease in the reduced thickness d of the c-domains in the case of a given relative thickness L of a stack of poly-twinned plates (see, e.g., Fig. 4 in Ref. 36).

An analysis of the calculations of $D(L)$ for small plates shows that the discontinuous variation in the period of the domain structure is due to the existence of two energetically stable magnetic states of a twinned system. One of them corresponds to the minimum of the magnetostatic energy, and the other to the minimum of the boundary energy. Whereas the minimum of the magnetostatic energy always occurs for $\tau = 0.5$, the contribution of the energy of the domain walls to the total energy of the crystal depends strongly on the size of the c-domains and of the poly-twinned plates. If 180° macrodomain walls disappear or if new ones are created the boundary energy changes as the macrodomain walls move driven by the change in the dimensions of the structural elements. The appearance of additional walls in large poly-twinned plates causes little change in the total area of the macrodomain walls, and therefore for the most part the features of the internal structure of the plates show up for the case of small L, comparable to d.

In order of magnitude the theoretical width of the macrodomains calculated for the FePt alloy corresponds to that observed experimentally. However, for a quantitative check on the theoretical calculations it is necessary to make a thorough study of the relation between the parameters of the domain structure and the dimensions L and d for specifically prepared samples containing only a single system of poly-twinned plates. Also required is a theoretical modeling of a complex domain structure of poly-twinned systems, in particular, an analysis of model (2) (Fig. 21b) should be carried out.

6.2. Single-domain nature of poly-twinned crystals

The usual definition of the critical size for a single domain as being the dimension below which the stable state of the crystal-particle is a uniformly magnetized state is not applicable to a poly-twinned crystal. At the same time, if in the first approximation a system can be regarded as a magnetically independent region, whose dimensions determine the parameters of the domain structure, it should be assumed that beginning at some size L_c the existence of macrodomain walls in a twinned particle will be energetically unfavorable.

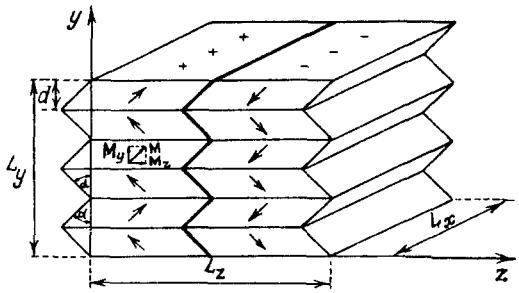

FIG. 23. Shape and characteristic dimensions of a particle consisting of crystalline c-domains. The fine lines indicate the boundaries of the c-domains and the Neél microdomain walls coincident with them. The heavy line indicates the 180° Bloch macrodomain wall.

It is logical to consider this size, below which the macrodomain state is realized, as the critical size for a single-domain poly-twinned crystal. In Ref. 38 the critical size L_c has been defined from the condition of equality of the total energy of a single-domain state, $F^{(1)}$, and a two-domain state, $F^{(2)}$, of a twinned particle. The total energy $F^{(1)}$ of a single-domain state is equal to the sum of the magnetostatic energy and the energies of the microdomain Neél walls. In a two-domain particle there are, in addition to these energies, additional contributions to the total energy from the energy of the 180° Bloch wall that divides the crystal into two macrodomains and from the energy of the magnetic $B-N$ regions of intersection of the Bloch and Neél walls.

To facilitate the calculations of the magnetostatic energy we assume that the twinned particle has the shape shown in Fig. 23. The side faces of the individual c-domains that form the twinned particle are inclined to the junction plane of the c-domains by an angle of $\pi/4$. Given that the c-domains have the same thickness and are arranged in pairs in the twinned particle, the magnetic charges on the upper and lower bases of the prism are arranged one on top of the other. In this case the intrinsic magnetostatic energy of a particle with dimensions L_x, L_y, and L_z is equivalent to the magnetostatic energy of a particle with the shape of a rectangular prism of the same dimensions but with the magnetization **M** along the y axis, and we can use the general expression for the magnetostatic energy.[44] Figure 24 shows, for a particle with a square base, $L_x = L_y = l$, the ratio of the intrinsic magnetostatic energy of the single-domain state to that of the two-domain state as a function of the relative dimension of the particle, L_y/L. For a cubic particle ($L_y/L = 1$) this ratio is 1.95; that is, the intrinsic magnetic energy of a two-domain particle is about half that of the single-domain state.

The expressions for the surface energy density of Neel domain walls and of the $B-N$ intersection region used in the calculation are given above [formulas (1), (2), (8), and (9)]. For the total energy of the magnetic domain walls of a single-domain, $F_\gamma^{(1)}$, and a two-domain, $F_\gamma^{(2)}$, twinned particle, taking into account the energy of the $B-N$ lines we have

$$F_\gamma^{(1)} = (2n-1)\gamma_N^{2\alpha} L_x L_z, \tag{18}$$

$$F_\gamma^{(2)} = \{(2n-1)(L_z - \pi\delta_0)\beta_N\gamma_\varphi + \frac{2\gamma_B}{\sin 2\alpha}[L_y \sin\alpha - 2(2n-1)\alpha\delta_\varphi] + \pi(2n-1)\lambda_{B-N}^{2\alpha}\delta_\theta\gamma_\varphi\} L_x, \tag{19}$$

$$\lambda_{B-N}^{2\alpha} = \left[\frac{\alpha}{\sin\alpha}\tanh\frac{\pi}{2} + \left(\frac{\pi}{2} - \tanh\frac{\pi}{2}\right) \times \sin^2\alpha \frac{\tanh(\alpha/\sin\alpha)}{1+\cos\alpha\tanh(\alpha/\sin\alpha)}\right],$$

$$\beta_N = 1 - \cos\alpha, \quad \gamma_\varphi = 4K\delta_\varphi. \tag{20}$$

The rest of the notation is defined in Sec. 4.1 and 4.3.

Depending on the relative size L_x/δ_0 of a particle for a specified number n of pairs of c-domains and a value of the parameter $\eta = 2\pi M_s^2/K$, the total energy $F^{(1)} = f_m^{(1)} + F_\gamma^{(1)}$ can be greater or less than the total energy $F^{(2)} = f_m^{(2)} + F_\gamma^{(2)}$. From the condition $F^{(1)} = F^{(2)}$, which states that the total energy of a macro-single-domain state is equal to that of a macro-two-domain state, we obtain the

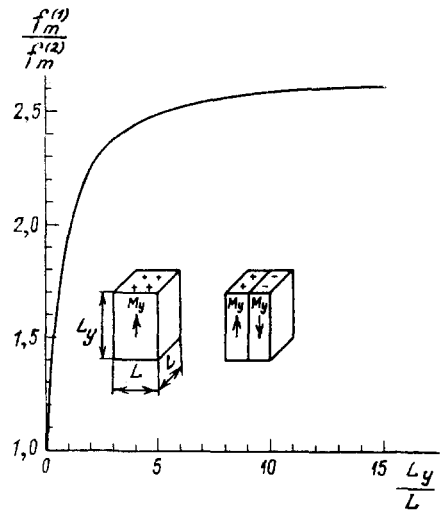

FIG. 24. Ratio of the intrinsic magnetostatic energy of a twinned particle in a single-domain to that in a two-domain state, $f_m^{(1)}/f_m^{(2)}$ as a function of the relative dimensions L_y/L ($L_x = L_z = L$).

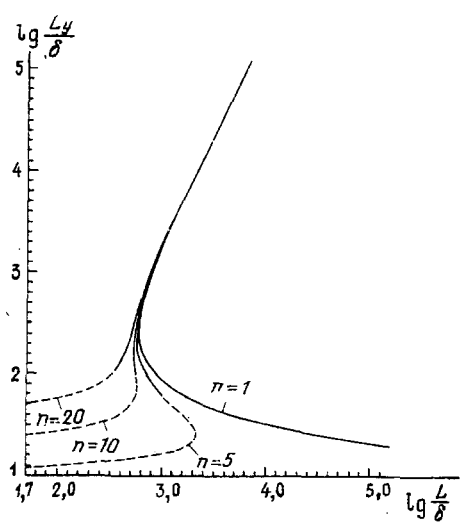

FIG. 25. Critical size for a single domain state, $L_c = L_y/\delta_0$ as a function of L/δ_0 for $\alpha = \pi/4$, $\eta = 0.1$ and various values of n. The dashed curves indicate regions of dimensions ξ_0 of the c-domains for which the approximation $\xi_0 > 5$ is not satisfied. For $n = 1$ this figure shows just the part of the curve that satisfies the condition $\xi_0 > 5$.

dependence of the critical size for a macro-single-domain for a twinned particle (for $\alpha = \pi/4$ and $A_1 = A_2$; see Sec. 4.3) as a function of the ratio of its dimensions and internal structure. Figure 25 shows this dependence for a particle with a square base ($L_x = L_y = L$) for the values $\eta = 0$ and 1 and $n = 1$, 5, 10, and 20. It can be seen that depending on the number of c-domains in a twinned particle, there can be from one to three critical sizes. As n is increased the number of critical values of L_y/δ_0 for a fixed L/δ_0 decreases and for sufficiently large n there is only one critical size. For $L_y/\delta_0 > 10^4$ all the curves coincide, regardless of the value of n. Consequently, for particle of such size the critical size for a macro-single-domain does not depend on the internal structure and is the same as that for ordinary homogeneous ferromagnets.

It is interesting to compare the data obtained here with the results of a numerical calculation of the conditions for a single domain for uniform uniaxial particles, as derived by Craik.[45] A comparison of the magnetic states of twinned and single-crystal particles with the same external geometrical dimensions shows that in a twinned particle with a small number of c-domains ($n < 10$) the single-domain state is stable for larger dimensions than in single crystals. This conclusion is important in the practical use of alloys of the CoPt type for permanent magnets.

7. CONCLUSIONS

Ferromagnetic alloys that become ordered with the formation of a poly-twinned microstructure are widely used magnetic materials whose potential is far from exhausted. Nonetheless, a theory of the magnetization processes, the hysteresis properties, and the magnetic domain structure of these alloys has only recently begun to be developed. In our investigations we have obtained new results for the physics of magnetic domains. They are the following:

1. It has been shown that an ordered microdomain magnetic structure is associated with the ordered crystallographic microstructure of poly-twinned systems. Two types of microdomain structures corresponding to two types of quasisaturated states are distinguished in a stack of poly-twinned plates.

2. A theory has been constructed for the various types of magnetic microdomain walls pinned at twin boundaries. The behavior of these "frozen-in" walls in a magnetic field has been analyzed.

3. We have introduced the concept of a cooperative magnetic domain structure, which consists of micro- and macrodomains. We have worked out an optical polarization method for observing the domains—a method by which is is possible to decipher and interpret the intricate pattern of the domain structure on surfaces with different crystallographic orientations. We have determined the principal features in the formation and behavior in a magnetic field of the cooperative domain structure of poly-twinned crystals with various degrees of dispersion of the structural elements.

4. We have proposed some models of cooperative magnetic domain structure that depend on the internal state and dimensions of the elements of the twinned system. We have obtained theoretically a qualitatively new formula for the dependence of the size of a microdomain on the size of a poly-twinned crystal. The multivalued and discontinuous nature of this dependence is due to the effect of the parameters of the crystal structure on the magnetic domain structure. For a calculation of the parameters of the domain structure a new entity must be introduced into the theory—the region of intersection of mobile macrodomains with "frozen-in" microdomain walls. The energy density of these unique "lines" is calculated.

5. We have introduced the concept of magnetic macro-single-domain state of a twinned crystal. The theory reveals a relation between the critical size for this property and the microstructure of the particle.

The hierarchy in the microstructure of ordered alloys (c-domains, blocks, plates, and stacks), which arises in the *fcc–fct* phase transition, corresponds to the hierarchy in the magnetic domain structure. The cooperative phenomena, i.e., self-organization, observed in the study of domain structure are due to exchange and magnetostatic interactions at the twin boundaries of the c-domains. They play an important role in the formation of the magnetic hysteresis properties of ordered alloys. The exchange and magnetostatic interactions induce the formation of metastable magnetic states and an increase in the effective size of the magnetically independent regions of ordered phase. These regions are not the individual c-domains, but regular systems of them. In the first approximation the poly-twinned plates and the blocks of c-domains or groups of them can be considered as a grain in a polycrystalline material. The existence of metastable magnetic states allows us to treat these grains as magnetically multiaxial.

Our observations have shown that during magnetization reversal the boundaries of these grains act as active centers for the formation of domains of reversed magnetization. Therefore, in alloys consisting of large stacks of poly-twinned plates, the macro-single-domain state is very unstable, and consequently the magnetic hysteresis characteristics are very weak. More pronounced hysteresis properties are obtained only in alloys with a highly dispersed twinned microstructure. In dispersed grains—blocks of c-domains smaller than the critical size for the grain to exist as a macro-single-domain, the macrodomain magnetic structure is absent in the residually magnetized state. The relative residual magnetization of poly-twinned crystals is also enhanced over that of polycrystalline material consisting of dispersed uniaxial grains by the exchange interaction at the twin boundaries of the c-domains. The dependence of the critical size for single-macro-domains on the external magnetic field also plays an important role in increasing the coercive force of alloys with a highly dispersed twin microstructure.

The theory we have developed for the domain structure and the hysteresis properties of poly-twinned crystals, which involves models of the rotation of the magnetization and the motion of macrodomain walls, predicts and explains, to a greater or lesser degree, the experimentally observed behavior of cooperative domain structure and the origin of the hysteresis properties. However, for a complete and well-grounded description of such complicated self-organizing systems as ferromagnetic poly-twinned crystals, apparently approaches are needed that are developed on the basis of modern synergetics.

[1] P. Brissonneau, A. Blanchard, and H. Bartholin, IEEE Trans. Magnetics **TM-2**, 479 (1966).
[2] Ya. S. Shur, L. M. Magat, G. V. Ivanova, A. I. Mitsek, A. S. Ermolenko,

and O. A. Ivanov, Fiz. Met. Metalloved. **26**, 241 (1968) [Phys. Met. Metallogr. (USSR) **26** (2), (1968)].
[3] O. A. Ivanov, L. V. Solina, V. A. Demshina, and L. M. Magat, Fiz. Met. Metalloved. **35**, 92 (1973) [Phys. Met. Metallogr. (USSR) **35**, (1) 81 (1973)].
[4] L. M. Magat, A. S. Ermolenko, G. V. Ivanova, G. M. Makarova, and Ya. S. Shur, Fiz. Met. Metalloved. **26**, 241 (1968) [Phys. Met. Metallogr. (USSR) **26** (3) (1968).
[5] P. Brissonneau and M. Schlenker, C. R. Acad. Sci. B (France) **264**, 282 (1967).
[6] J. M. Pennisson, A. Bourret, and Ph. Eurin, Acta Met. **19**, 1195 (1971).
[7] N. N. Shchegoleva, L. M. Magat, and Ya. S. Shur, Fiz. Met. Metalloved. **34**, 663 (1972). [Phys. Met. Metallogr. (USSR) **34** (3), 211 (1972)].
[8] G. Hadjipanayis and P. Gaunt, J. Appl. Phys. **50**, 2358 (1979).
[9] V. A. Ivchenko, E. I. Teitel' and N. N. Syutkin, Fiz. Met. Metalloved. **52**, 164 (1981) [Phys. Met. Metallogr. (USSR) **52** (1), 140 (1981)].
[10] V. D. Plakhtiĭ and Yu. D. Tyapkin, Metallofizika **6**, 88 (1984). [Phys. Met. (GB) **6** (4), 803 (1985)].
[11] N. N. Shchegoleva, L. M. Magat, and Ya. S. Shur, Fiz. Met. Metalloved. **39**, 528 (1975) [Phys. Met. Metallogr. (USSR) **39** (3), 70 (1975)].
[12] N. I. Sokolovskaya, N. N. Shchegoleva, and G. S. Kandaurova, Fiz. Met. Metalloved. **41**, 55 (1976) [Phys. Met. Metallogr. (USSR) **41** (1), 42 (1976)].
[13] N. I. Vlasova, N. N. Shchegoleva and Ya. S. Shur, Fiz. Met. Metalloved. **58**, 676 (1984) [Phys. Met. Metallogr. (USSR) **58**, (4), 43 (1984)].
[14] E. S. Yakovleva, V. I. Syutkina, and O. D. Shashkov, *Phase Transitions in Metals and Alloys* [in Russian], in Papers of the Ural Scientific Center, Academy of Sciences of the USSR, Sverdlovsk (1975), p. 57.
[15] G. V. Ivanova, L. M. Magat, L. V. Solina, and Ya. S. Shur, Fiz. Met. Metalloved. **32**, 543 (1971) [Phys. Met. Metallogr. (USSR) **32** (3), 92 (1971)].
[16] G. S. Kandaurova, L. G. Onoprienko, and B. D. Vorontsov, Fiz. Met. Metalloved. **41**, 702 (1976) [Phys. Met. Metallogr. (USSR) **41** (4), 22 (1976)].
[17] L. G. Onoprienko, Fiz. Met. Metalloved. **44**, 7 (1977) [Phys. Met. Metallogr. (USSR) **44** (1), 1 (1977)].
[18] L. G. Onoprienko, G. S. Kandaurova, and N. I. Vlasova, *Physical Properties of Magnetic Materials* [in Russian], Papers of the Institute of Metal Physics, Ural Scientific Center, Academy of Sciences of the USSR, Sverdlovsk (1982), p. 68.
[19] L. G. Onoprienko, G. S. Kandaurova, and B. D. Vorontsov, Fiz. Met. Metalloved. **47**, 89 (1979) [Phys. Met. Metallogr. (USSR) **47** (1), 70 (1979)].
[20] G. S. Kandaurova, L. G. Onoprienko, and N. G. Sokolovakaya, Phys. Status. Solidi A, **73**, 351 (1982).
[21] V. A. Tsurin, A. E. Ermakov, Yu. G. Lebedev, and B. N. Filippov, Phys. Status. Solidi A **33**, 325 (1976).
[22] N. I. Sokolovskaya, G. S. Kandaurova, B. D. Vorontsov, and L. G. Onoprienko, Fiz. Met. Metalloved. **37**, 762 (1974) [Phys. Met. Metallogr. (USSR) **37** (4), 75 (1974)].
[23] N. I. Sokolovskaya, G. S. Kandaurova, L. G. Onoprienko, and B. D. Vorontsov, Fiz. Met. Metalloved. **39**, 207 (1975) [Phys. Met. Metallogr. (USSR) **39** (1), 187 (1975)].
[24] B. D. Vorontsov, G. S. Kandaurova, L. G. Onoprienko, and N. I. Sokolovskaya, Fiz. Met. Metalloved. **44**, 1163 (1977) [Phys. Met. Metallogr. (USSR) **44** (6), 33 (1977)].
[25] J. B. Newkirk, R. Smolochowsky, A. H. Geisler, and D. L. Martin, J. Appl. Phys. **22**, 290 (1951).
[26] A. G. Khachaturyan, *Theory of Structural Phase Transitions of Solid Solutions* [in Russian], Nauka, M. (1974), pp. 286–299.
[27] A. L. Roitburd, Usp. Fiz. Nauk **113**, 69 (1974) [Sov. Phys. Usp. **17**, 326 (1974)].
[28] D. J. Craik, in *Magnetic Structure of Ferromagnets* (1959). Proc. Phys. Soc. London **69**, 647 (1956) [Russ. transl., IL, M., 1959, p. 137].
[29] W. Pepperhoff, Arch. Eisenhuttenwes. **34**, 767 (1963).
[30] A. V. Sokolov, *Optical Properties of Metals*, Blackie, London, 1961. [Russ. original, Fizmatgiz, M. 1965].
[31] N. I. Vlasova, *Domain structure and magnetic properties of alloys with twinned microstructure* [in Russian], Dissertation, Candidate of Physical and Mathematical Sciences, Institute of Metal Physics, Ural Branch, Academy of Sciences of the USSR, Sverdlovsk, 1989.
[32] G. Dedié, J. Niemeyer, and Ch. Schwink, Phys. Status. Solidi B, **43**, 163 (1971).
[33] G. S. Kandaurova and Yu. V. Ivanov, Zh. Eksp. Teor. Fiz. **70**, 666 (1976) [Sov. Phys. JETP **43**, 343 (1976)].
[34] Z. Malek and V. Kambersky, Czech. J. Phys. **8**, 416 (1958).
[35] N. I. Vlasova, N. N. Shchegoleva, and Ya. S. Shur, Fiz. Met. Metalloved. **63**, 463 (1987) [Phys. Met. Metallogr. (USSR) **63** (3), 40 (1987)].
[36] L. G. Onoprienko, G. S. Kandaurova, and N. I. Vlasova, Fiz. Met. Metalloved. **63**, 837 (1987) [Phys. Met. Metallogr. (USSR) **63** (5), 1 (1987)].
[37] L. G. Onoprienko and N. I. Vlasova, Fiz. Met. Metalloved. **53**, 510 (1982) [Phys. Met. Metallogr. (USSR) **53** (3), 89 (1982)].
[38] L. G. Onoprienko, G. S. Kandauova, and N. I. Vlasova, Fiz. Met. Metalloved. **64**, 54 (1987) [Phys. Met. Metallogr. (USSR) **64** (1), 46 (1987)].
[39] G. S. Kandaurova, L. G. Onoprienko, and N. I. Vlasova, Fiz. Met. Metalloved. **64**, 1061 (1987) [Phys. Met. Metallogr. (USSR) **64** (6), 16 (1987)].
[40] M. Ya. Shirobokov, Zh. Eksp. Teor. Fiz. **15**, 57 (1945); Zh. Eksp. Teor. Fiz. **16**, 61 (1946).
[41] N. I. Vlasova and Ya. A. Shur, Fiz. Met. Metalloved. **63**, 702 (1987) [Phys. Met. Metallogr. (USSR) **63** (4), 69 (1987)].
[42] A. I. Mitsek and V. N. Pushkar', *Real Crystals with Magnetic Ordering* [in Russian], Naukova Dumka, Kiev, 1978.
[43] Yu. N. Dragoshanskiĭ and Ya. S. Shur, Fiz. Met. Metalloved. **21**, 678 (1966) [Phys. Met. Metallogr. (USSR) **21** (5), (1966)].
[44] J. B. Goodenough, Phys. Rev. **102**, 356 (1956) [Russ. transl., IL, M., 1959, p. 58].
[45] D. J. Craik and D. A. McIntyre, Proc. R. Soc. London Ser. A **302**, 99 (1967).

Translated by J. R. Anderson